Thermomechanical couplings in elastomers: contributions of surface calorimetry by imaging

J.-B Le Cam

Couplages dans les matériaux élastomères : apport de la calorimétrie de surface par imagerie

J.-B. Le Cam

Univ Rennes, CNRS, IPR (Institut de Physique de Rennes) - UMR 6251
35000 Rennes, France

Résumé : ce document de synthèse, rédigé en anglais, traite de l'usage de la calorimétrie de surface pour *étudier les mécanismes de déformation et d'endommagement dans les élastomères*. Il s'appuie principalement sur un ouvrage de synthèse[111] et un article[105] récemment publiés, qui abordent, entre autres, la détermination et l'analyse de champs calorimétriques sous chargements mécaniques engendrant de grandes déformations homogènes et hétérogènes.
L'introduction évoque brièvement l'histoire de cette thématique : les travaux pionniers sur la caractérisation du comportement énergétique des matériaux métalliques au début du siècle dernier, la genèse de la calorimétrie sous étirement des élastomères dans les années 70, les approches de *calorimétrie de surface en thermomécanique des matériaux* développées depuis la fin des années 80 et pour finir, *leur extension aux grandes déformations*, en particulier pour la caractérisation de champs calorimétriques de surface hétérogènes.
La première partie du document introduit le *cadre théorique permettant de quantifier la réponse calorimétrique à partir de champs thermiques et de l'équation de diffusion de la chaleur en grandes déformations*. La méthodologie permettant d'établir les bilans d'énergie et de mesurer la cristallinité induite sous déformation est également détaillée. Le document aborde ensuite les expérimentations type, en présentant les différentes géométries d'éprouvettes, les conditions de chargement et les choix méthodologiques relatifs à l'instrumentation et au traitement des images. *Les réponses calorimétriques caractéristiques des élastomères sont présentées à partir de l'étude de quatre matériaux*, spécifiquement formulés afin d'activer ou, au contraire, d'inhiber les différents couplages thermomécaniques, ainsi que la production de dissipation intrinsèque. Ceci permet de distinguer plusieurs familles de comportement calorimétrique, en fonction de l'utilisation ou non de charges renforçantes et de la capacité des matériaux à cristalliser sous étirement. *Une illustration de l'intérêt d'établir des bilans d'énergie globaux est donnée par une classification de matériaux élastomères en fonction de leur comportement énergétique*, qui traduit leur plus ou moins grande capacité à stocker de manière réversible de l'énergie mécanique. Le document s'achève par une *ouverture sur le traitement de champs calorimétriques hétérogènes, en distinguant les hétérogénéités dues aux effets géométriques de celles induites par le matériau lui-même*. Cette dernière partie expérimente ainsi le potentiel des approches calorimétriques pour l'identification locale des paramètres constitutifs, l'étude du fonctionnement thermomécanique des zones en pointe de fissures et la mise en évidence des hétérogénéités du matériau.

Thermomechanical couplings in elastomers: contributions of surface calorimetry by imaging

J.-B. Le Cam

Univ Rennes, CNRS, IPR (Institut de Physique de Rennes) - UMR 6251
35000 Rennes, France

Abstract: this review paper, written in English, addresses the use of surface calorimetry *to investigate deformation and damage mechanisms in elastomers*. It is mainly based on a recently published review book[111] and article[105], which discuss, among other aspects, the determination and analysis of calorimetric fields under mechanical loadings producing large homogeneous and heterogeneous deformations.
The introduction briefly outlines the historical development of this research field. It recalls the pioneering work carried out at the beginning of the last century on the energetic behavior of metallic materials, the emergence of elastomer calorimetry under stretching in the 1970s, the development of *surface calorimetry approaches in thermomechanics of materials* since the late 1980s, and finally *their extension to large deformations*, particularly for the characterization of heterogeneous surface calorimetric fields.
The first part of the document introduces the *theoretical framework required to quantify the calorimetric response from thermal fields and the heat diffusion equation in the context of large deformations*. The methodology used to establish energy balances and to measure strain-induced crystallinity is also detailed. The document then describes typical experimental procedures, presenting the different specimen geometries, loading conditions, and methodological choices related to instrumentation and image processing.
Characteristic calorimetric responses of elastomers are illustrated through the study of four materials specifically formulated either to activate or to inhibit various thermomechanical couplings, as well as the production of intrinsic dissipation. This approach makes it possible to distinguish several families of calorimetric behavior depending on the presence or absence of reinforcing fillers and on the ability of the materials to crystallize under stretching. *The relevance of establishing global energy balances is further illustrated through a classification of elastomeric materials according to their energetic behavior*, reflecting their respective ability to reversibly store mechanical energy.
Finally, the document concludes with a *perspective on the analysis of heterogeneous calorimetric fields, distinguishing heterogeneities arising from geometric effects from those induced by the material itself*. This last section highlights the potential of calorimetric approaches for the local identification of constitutive parameters, the investigation of the thermomechanical behavior in crack-tip regions, and the identification of material heterogeneities.

1. Introduction

During deformation, materials release or absorb heat as a result of both reversible mechanisms, including energetic and entropic elasticity, as well as latent heat associated with solid–solid phase transitions and irreversible mechanisms, such as viscous effects, plastic deformation, and damage processes like cavitation, crack propagation, and aging. The relative contribution of these mechanisms strongly depends on the nature of the material and the applied loading conditions. Consequently, analysing deformation through thermal and calorimetric responses provides information that complements conventional mechanical measurements and facilitates a deeper understanding of the links between microstructural evolution and thermomechanical behavior. This helps chemists, physicists and mechanicians to better link microstructure and thermomechanical properties. *Since the early twentieth century, extensive investigations have been devoted to metallic materials within this framework, particularly in relation to plastic deformation. Landmark studies by Farren and Taylor[1] and later by Taylor and Quinney[2] quantified the latent energy remaining after plastic deformation through "cold working" in a metal under quasi-static monotonous loadings. These works introduced the concept of a ratio, describing the proportion of anelastic deformation energy rate irreversibly converted into heat, and now widely known as the Taylor–Quinney coefficient[3-7]. Their analyses demonstrated that a significant fraction of the mechanical work supplied during deformation is stored in the microstructure, leading to an increase in internal energy rather than being fully converted into heat.*

In their review dedicated to the stored energy of cold work, Bever et al[8] explained that under certain favorable conditions, cold-worked metals undergo recovery processes during which part of the stored energy can be released. Such findings are particularly relevant for improving the understanding of energy storage and dissipation mechanisms in elastomeric materials. Implementing a thermodynamic description of deformation requires accurate temperature measurements, which are affected by heat conduction within the material as well as heat exchanges with the surrounding environment and the testing apparatus. Even when experiments are conducted under adiabatic conditions at the scale of the tested specimen, pronounced temperature gradients can arise locally, leading to non-negligible heat diffusion by conduction, most notably in highly stressed regions such as crack tips in stretched specimens. For this reason, the analysis of heat source fields is generally preferred over temperature measurements when investigating thermomechanical behavior[9-12].

Although to a lesser extent than metals, polymers have also been studied using calorimetric techniques. Notable examples include the work of Rittel and Rabin[13] on heat generation during cyclic loading of two glassy polymers, and studies by Chrysochoos and co-workers on the kinetics of stored and dissipated energy in polyamide 6.6 under cyclic loading[14], as well as the influence of the relative humidity and loading frequency on its thermomechanical cyclic response[15]. Despite the relevance of these approaches, calorimetric investigations of stretched rubbers remain limited, even though natural

rubber (NR) was among the first materials for which thermosensitivity was identified as early as the nineteenth century by Gough[16] (1805) and Joule[17] (1857).[i] Indeed, most experimental studies on rubbers throughout the twentieth century primarily focused on mechanical behavior, see studies on the stress softening initiated as early as 1903 by Bouasse and Carrière,[19] and continued by Holt[20] and Mullins[21]; studies on the fatigue properties of carbon black filled NR with the pioneering work of Cadwell et al[22] and Fielding[23] for crack initiation, and Rivlin and Thomas,[24] and Thomas[25] for crack growth resistance.

From the 1970s onward, the mechanics of elastomers has focused more on behavior modeling than on the physical phenomena of deformation, which made numerical simulation and structural design possible with the advent of computational mechanics in the 1980s. However, physically based models would greatly benefit from a more thorough understanding of deformation and damage mechanisms, particularly in relation to topics such as fatigue life enhancement in crystallizing rubbers,[22,26,27] the origin and significance of mechanical hysteresis,[28] and the temperature dependence of the mechanical response.[29]

The first calorimetric investigations of elastomer deformation were not reported until the early 1970s, notably through the work of Göritz and co-workers (see for example Ref. 30). Using a stretch calorimeter, they demonstrated that the thermal energy associated with strain-induced crystallization (SIC) could be quantitatively measured. Since crystallization is a highly exothermic process, the degree of crystallinity can be directly inferred from the contribution to the total heat source solely attributed to SIC, providing a simpler alternative to X-ray diffraction techniques[ii]. Despite this potential, stretch calorimetry was subsequently abandoned as a tool for crystallinity assessment and for studying deformation mechanisms in rubbers. Among the possible reasons is the fact that the measurement is made at the scale of the specimen and not at the local scale. The point is that the large and possibly heterogeneous strains experienced by rubbers make the local temperature measurement with a thermocouple impossible.

This is probably why the advent of infrared cameras has led to new calorimetric studies in the field of experimental thermomechanics of rubbers. This type of camera has also provided a wealth of information on thermal gradients in the presence of strong geometric singularities such as cracks.[32] Before going any further, it is worth focusing on the concept of the rubber elasticity, which is often considered as an entropy-driven elasticity. Nevertheless, deviations to this theory have been experimentally evidenced by several authors, see for example Allen and coauthors,[33-35] Shen[36] and Shen and Croucher.[37] As detailed and discussed by Treloar in Refs 38 and 39, non-entropic (energetic) effects also contribute to rubber elasticity. They are due to change in the network chain conformations, which affects the intramolecular internal energy. This is confirmed by the fact that the energetic contribution to rubber elasticity does not change when diluents are

[i] even before Clausius introduced the concept of entropy (page 391 in Ref. 18.)

[ii] It should be noted that the crystallinity measurement with different techniques than the XRD was investigated as soon as 1968 from temperature measurement by Mitchell and Meier[31].

incorporated.[40] Change in the chain packing may also affects the intermolecular internal energy. Therefore, both energetic and entropic elasticity contribute to the elastic reaction force. In addition to the book written by Treloar,[39] the reader can refer to Refs. 41 to 44 to find out more about experimental and theoretical thermodynamics of elastomers.

In 2006, Honorat reported the first surface calorimetric characterization of cyclic deformation of an unfilled NR using infrared thermography under relaxing and non-relaxing uniaxial tensile loading.[45] He showed the competition between entropic and non-entropic (energetic) elasticity in the calorimetric response and proposed a simple model capable of predicting the thermoelastic inversion phenomenon.[17-46] Caborgan completed the work by Honorat using the same technique and applying a larger number of deformation cycles.[47] In the same period, Samaca Martinez et al carried out an exhaustive study on the calorimetric signature of the phenomena involved in the rubber deformation: the nature of the elasticity,[48] the viscosity,[49] the stress softening induced by fillers[50] and the crystallization.[48] A summary is proposed in Refs 51 and 52.

Finally, Lachhab et al[53] and Loukil et al[54] introduced an energetic ratio, denoted γ_{se}, which quantifies the fraction of mechanical energy stored and released during a thermodynamic cycle, respectively due to the crystallization/melting process in a polyurethane and by the filler network in a nitrile rubber. This ratio highlights that the part of the hysteresis loop in rubbers is not systematically due to viscosity or damage. In addition, pushing forward the processing of the heat source, Le Cam[55] proposed to couple the work by Göritz and co-workers on stretch calorimetry and the IR thermography-based surface calorimetry approach to evaluate the strain-induced crystallinity in an unfilled NR. The method was then successfully validated by comparison with the XRD technique by Le Cam et al.[56] Recently the measurement has been extended to NR filled with different carbon black filler types in Le Cam et al[57] and to the characterization of heterogeneities in the strain-induced crystallinity fields.[58]

The above-mentioned studies deal with homogeneous tests. It should be noted that only a few studies have investigated the calorimetric response obtained during heterogeneous tests. Moreover, they have very different objectives: inverse identification of the constitutive parameters without using (measuring) boundary conditions,[59] characterization of the effect of the multiaxial strain state on the calorimetric response with a 3-branch specimen[60] and a cruciform specimen,[61] investigation of the calorimetric behavior of the crack tip zone where the mechanical field is highly heterogeneous.[62-65]

This document is organized as follows. In Section 2, the thermodynamic framework of the surface calorimetry in the case of large deformations is presented. The results presented in Sections 3 and 4 summarize the results mainly derived from work conducted with our group at Institute of Physics Rennes (University of Rennes, France). Section 3 recalls the typical experimental setups used (specimen geometries, loading conditions, imaging techniques) and, more importantly, the experimental precautions required. The results obtained are presented in Section 4. They show that several families can be distinguished in terms of the calorimetric response, depending on whether the material is filled or not, crystallizing or not. Finally, the document concludes with a forward-looking

analysis of the treatment of heterogeneous calorimetric fields, clearly distinguishing heterogeneities originating from geometric effects from those inherent to the material. This concluding section underscores the potential of calorimetric approaches for the local identification of constitutive parameters, for the investigation of the thermomechanical response in regions exhibiting strong singularities such as crack tips, and for the characterization of material when establishing links between microstructure and thermomechanical properties at the macroscopic scale.

2. Theoretical framework for quantitative surface calorimetry

Surface calorimetry consists in determining the heat power density, commonly referred to as the heat source, by combining temperature measurements acquired at the material surface with the heat diffusion equation. The term "heat source reconstruction" is frequently used to stand for this approach. When thermal data are obtained as a two-dimensional field, as is typically the case with infrared (IR) thermography on a flat surface, the general three-dimensional heat diffusion formulation must be appropriately simplified to process the thermal measurement. The methodological approach adopted in this section follows the theoretical developments originally introduced in Ref. 61.

In the case where the constitutive state equations are derived from the Helmholtz free energy function and the heat conduction follows Fourier's law, the formulation of the local heat diffusion equation writes as follows with respect to the reference configuration (corresponding here to the undeformed state):

$$\boldsymbol{\rho_0 C\dot{T} + DivQ - R = \underbrace{\mathcal{D}_{int} + T\frac{\partial P}{\partial T}:\dot{F} + T\frac{\partial A_\beta}{\partial T}:\dot{\xi}_\beta}_{\widehat{S}}} \quad (1)$$

with $\boldsymbol{\rho_0}$ the initial mass density, $\boldsymbol{C}$ the heat capacity, $\boldsymbol{T}$ the absolute temperature, $\boldsymbol{Q}$ the heat influx per unit reference area, $\boldsymbol{R}$ the external heat source (due to radiation, for instance), $\boldsymbol{F}$ the deformation gradient tensor, $\boldsymbol{P}$ the first Piola-Kirchhoff stress tensor (or nominal stress tensor) and $\boldsymbol{\mathcal{D}_{int}}$ the intrinsic dissipation (also named mechanical dissipation). $\widehat{\boldsymbol{S}}$ denotes the heat source. Div is the divergence operator calculated according to the reference (Lagrangian) configuration. The superposed dot stands for the material time derivative. Note that $\boldsymbol{Q = -det(F)F^{-1}K_0F^{-T}GradT}$, where $\boldsymbol{K_0}$ is the thermal conductivity tensor. The term $\boldsymbol{T\frac{\partial P}{\partial T}:\dot{F}}$ corresponds to the heat sources due to the coupling between strain and temperature, which origin can be entropic and or energetic. The term $\boldsymbol{T\frac{\partial A_\beta}{\partial T}:\dot{\xi}_\beta}$ represents the other thermomechanical couplings, where $\boldsymbol{\xi_\beta}$ are the internal variables and $\boldsymbol{A_\beta}$ the corresponding thermodynamic forces.

2.1. Simplification of the heat diffusion equation

2.1.1. 2D formulation

IR cameras provide two-dimensional thermal fields. Reconstructing the two-dimensional heat source field from these fields requires therefore the formulation of a two-dimensional version of the heat diffusion equation. In this approach, several assumptions are made: (i) the material is incompressible (ii) the temperature is constant over the specimen thickness[iii] (iii) the heat conduction is isotropic. The specimen is therefore thin and the plane stress state can be generally assumed. Under such conditions, Eq. (1) can be integrated over the thickness, which leads to the two-dimensional formulation of the heat diffusion equation:

$$\rho_0 C\left(\dot{T}+\frac{T-T_{amb}}{\tau_{2D}}\right)-\mathrm{Div}_{2D}(k_0\mathbf{C^{-1}}\mathrm{Grad}_{2D}T)-R=\hat{S}, \tag{3}$$

where T_{amb} is the ambient temperature. k_0 is the thermal conductivity coefficient. $\mathbf{C}=\mathbf{F^T F}$ is the right Cauchy-Green tensor. Div_{2D} and Grad_{2D} are respectively the divergence and gradient operators in the specimen plane calculated according to the reference (Lagrangian) configuration. τ_{2D} is a time representing the heat exchanges by convection with the air at the specimen surface along the thickness direction. This equation is obtained under assumptions that may be strong and even unrealistic, depending on the material properties and specimen's geometry tested. The experiment must therefore be carefully assessed beforehand in light of these assumptions, which could lead to additional measurements (typically the volume change) or numerical simulation (if thermophysical properties change along the thickness direction).

By considering the temperature variation $\theta(X,Y,t)=T(X,Y,t)-T_{ref}(X,Y)$ instead of the temperature itself, the heat diffusion equation can be written without the external radiations R if they are constant during the deformation process. It should be noted that T_{ref} is the ambient temperature if it is constant over the test. In this case, Eq. (3) writes:

$$\rho_0 C\left(\dot{\theta}+\frac{\theta}{\tau_{2D}}\right)-\mathrm{Div}_{2D}(k_0\mathbf{C^{-1}}\mathrm{Grad}_{2D}\theta)=\hat{S}. \tag{4}$$

[iii] This assumption can be verified for the test configuration considered by calculating the Biot number B_i. This number is the ratio between the thermal resistance for conduction inside a body and the resistance for convection at the surface of the body. It characterizes how significant the temperature inside a body varies in space when the body is submitted to a heat flux at its surface. In the case of a rectangular thin specimen:

$$B_i=\frac{h}{k_0}.\frac{e}{2} \tag{2}$$

where h is the convection coefficient, k_0 is the thermal conductivity coefficient, and e is the thickness. If $B_i<0.1$, the temperature variation in the thickness is less than 5%,[66] which is typically the case for a 2 mm thick rectangular rubber specimen.

This two-dimensional formulation of the heat diffusion equation has recently been applied to the thermomechanical characterization of moderate heterogeneities in the mechanical strain state[59,60] or strong ones in the influence zone of crack tips in rubber specimens.[62,65]

To apply Eq. (4), τ_{2D} has to be characterized according to the stretch λ, defined as the ratio of the current length to the initial length in the stretch direction, and the biaxiality coefficient B, as defined in Refs 67 and 68. In other words, as τ varies spatially according to the change in the thickness, i.e., to the stretch λ and to the biaxiality ratio B, $\tau_{2D} = \tau(\lambda, B)$. $\tau(\lambda, B)$ can be assessed in two different ways:

- by heating (or cooling) the specimen and measuring the temperature field during the return to thermal equilibrium, then by fitting the curves with an exponential function,
- by considering that the thickness changes are derived by assuming that the material is incompressible:

$$\tau(\lambda, B) = \tau_0 \lambda^{-B-1}. \quad (5)$$

τ_0 is the value of τ determined from the thermalization in the undeformed state.

The accurate evaluation of $\tau(\lambda, B)$ is all the more important that the test is performed at a low loading rate, which leads to significant heat diffusion by convection, and thus to small temperature variations. In Charlès and Le Cam[59] the two methods have been compared and a good correlation was found. Counterintuitively, measuring τ for different global stretches is not systematically the more accurate method. Typically, for stretches activating SIC in crystallizable rubbers, the return to the thermal equilibrium is disturbed by the competition between heat production due to recrystallization and heat diffusion due to convection.

2.1.2. "0D" formulation

In practice, for materials with low thermal diffusivity such as rubber, the only thermal gradient obtained under homogeneous loading is limited to the area near the grips, i.e., heat conduction in the specimen plane is negligible and heat exchanges with the grips of the testing machine does not induce temperature gradient in the measurement zone, generally in the specimen middle. This is also true for heterogeneous heat source fields if the diffusion length is small compared to the spatial resolution of the thermal measurement. In this case, the two-dimensional heat diffusion equation can be simplified[69,70] and would be a "0D"-like formulation of the heat diffusion equation:

$$\rho_0 C \left(\dot{\theta} + \frac{\theta}{\tau_{2D}} \right) = \hat{S}. \quad (6)$$

Such simplification has previously been done for metallic materials even under heterogeneous strain states,[9,12,71,72,73] and more recently applied for characterizing the

calorimetric signature of the different mechanisms in play in the homogeneous[45,47-57] and heterogeneous deformations[58,60] of rubber.

2.2. Energy balance

The calorimetric response accompanying the mechanical response gives access to a wide range of complementary information on the deformation mechanisms. In particular, the imbalance between the heat generated and the heat absorbed over a thermodynamic cycle allows the determination of the average intrinsic dissipation, corresponding to the mechanical energy converted into heat, which can be compared to the energy involved in the hysteresis loop. This provides therefore a direct evaluation of the mean intrinsic dissipation responsible for the self-heating. It is important to distinguish between two forms of dissipation: thermal dissipation, which arises from heat diffusion within the material and heat exchange with the surroundings, and intrinsic dissipation, which originates from irreversible deformation processes. Here, even though the test conditions are not adiabatic, the thermophysical properties of elastomers lead to a negligible contribution of the thermal dissipation to the hysteresis loop. This can be verified by integrating the term $\frac{\theta}{\tau_{2D}}$ over the cycle.

Intrinsic dissipation is defined as a power density, whereas the mean intrinsic dissipation represents an energy rate**.** For a detailed thermodynamic treatment of irreversible processes, the reader is referred to Ref. 74. Therefore, the difference between the energy involved in the hysteresis loop and the energy corresponding to the mean intrinsic dissipation identifies as the mechanical energy stored in the material due to thermomechanical couplings and that changes its internal energy.

The continuum quantities required for such an energy balance are listed below:

- The total strain energy density (per unit reference volume) W_{strain} is the energy supplied mechanically to the material during the loading W_{strain}^{load} and the unloading W_{strain}^{unload}:

$$W_{strain}^{load} = \int_{loading} \pi d\lambda \text{ and } W_{strain}^{unload} = \int_{unloading} \pi d\lambda, \text{respectively,} \qquad (7)$$

  where π denotes the first component of Piola-Kirchhoff stress tensor **P** in the loading direction and λ is the corresponding stretch. The calculation *de facto* applies to a uniaxial and homogeneous test.

- The mechanical energy involved in the hysteresis loop W_{hyst}^{cycle} and the corresponding energy rate P_{hyst}^{cycle} are determined as follows:

$$W_{hyst}^{cycle} = W_{strain}^{load} - W_{strain}^{unload}, \qquad P_{hyst}^{cycle} = \frac{W_{hyst}^{cycle}}{t_{cycle}} \qquad (8)$$

where t_{cycle} denotes the cycle duration.

- Integrating the heat source over time of each cycle gives the mean intrinsic dissipation $\widetilde{\mathcal{D}}_{int}$:

$$\widetilde{\mathcal{D}}_{int} = \frac{1}{t_{cycle}} \int_{cycle} \hat{S} dt \,. \tag{9}$$

- The difference between P_{hyst}^{cycle} and $\widetilde{\mathcal{D}}_{int}$ represents the energy stored rate P_{stored}^{cycle} during each cycle:

$$P_{stored}^{cycle} = P_{hyst}^{cycle} - \widetilde{\mathcal{D}}_{int}, \tag{10}$$

and the corresponding mean energy is therefore:

$$W_{stored}^{cycle} = P_{stored}^{cycle} \,.\, t_{cycle}. \tag{11}$$

- The stored energy ratio γ_{se} is defined as

$$\gamma_{se} = \frac{W_{stored}^{cycle}}{W_{hyst}^{cycle}} \tag{12}$$

and further characterizes the ability of the material to store energy:

- if γ_{se} tends to 0, no energy is stored during the deformation. The whole hysteresis loop is due to the intrinsic dissipation,
- if γ_{se} tends to 1, the whole hysteresis loop is due to stored energy and no intrinsic dissipation is detected. This is typically the case in unfilled natural rubber.[48] It should be noted in this this case that this energy is released with a different kinetics during the unloading.

This ratio can be influenced by both the strain range and the strain rate applied to the specimen.[54] Moreover, it is valid in the case where the thermal dissipation is negligible. Else, the mean thermal dissipation has to be removed from W_{stored}^{cycle}.

2.3. Strain-induced crystallinity evaluation

The strain-induced crystallinity of rubber is classically evaluated by the XRD technique, which has the advantage of providing additional information of importance on the crystalline phase structure,[75-78] chain orientation,[79] crystallization kinetics.[80-82] Since SIC is highly exothermic, alternative methods based on temperature or calorimetry measurements can be used to determine the crystallinity. To this end, a technique to evaluate the thermal energy and the corresponding temperature variation due to SIC (denoted ΔT_{cryst} in the following) from surface calorimetry has been proposed in Ref. 55, without using the mechanical response. The crystallinity is obtained by considering that the crystallization energy of natural rubber can be approximated by the fusion enthalpy

ΔH_{cryst}, which is assumed to be independent of temperature and stretch. As an example, the value determined by Trabelsi et al.[81] for the NR they used was equal to $59.9\ J.cm^{-3}$. The crystallinity can be expressed in terms of ΔT_{cryst} as follows:

$$\chi(t) = \frac{\rho C \Delta T_{cryst}(t)}{\Delta H_{cryst}} \tag{13}$$

For filled materials, this ratio has to be weighted by a factor $\frac{1}{1-\Phi_{filler}}$, where Φ is the filler volume fraction.

The methodology is briefly recalled by the diagram in Figure 1. It is composed of four steps:

- Step #1: the temperature variation $\theta(t)$ and parameter $\tau(\lambda)$ are processed with the 0D formulation of the heat diffusion equation to calculate the heat source.
- Step #2: the thermal energy due to SIC is determined from the area between the heat source measured and the heat source prediction due to coupling between temperature and strain only. The heat source prediction is carried out by fitting the heat source measured from stretches inferior to the SIC onset λ_c, the stretch at which SIC starts.
- Steps #3 and #4: the corresponding temperature variation due to SIC is calculated for a numerical integration scheme and the crystallinity is finally obtained with Eq. (13).

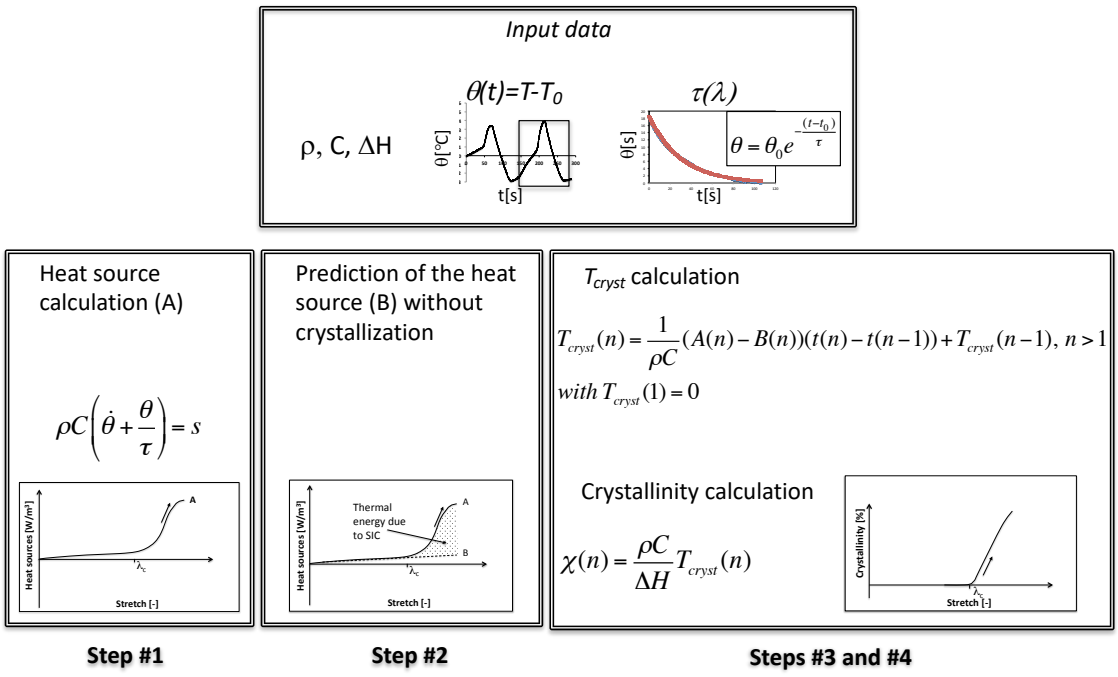

Figure 1: Methodology for evaluating the crystallinity from the calorimetric response

Results obtained with this method show very good agreement with those obtained with the XRD technique when applied to the same unfilled NR.[56]

Remark on the heat source prediction due to thermoelastic couplings only: *for unfilled NR, the thermal energy of SIC is well approximated whatever the polynomial chosen to predict the heat source due to thermoelastic couplings only. Indeed, the exothermal peak due to SIC is of high intensity and of narrow width, so the degree of the polynomial has very few effects on the prediction. Recently, Le Cam et al studied the crystallinity measurement in a NR unfilled and filled with different types of filler.[57] By comparison with XRD measurements, the authors showed that even the tangent to the heat source before SIC starts can be used in the case of unfilled NR. However, in the case of filled NR, the calorimetric response exhibits a lower in intensity and larger peak. Therefore, the degree of the polynomial chosen has a strong influence on the results. The authors demonstrated that the tangent or a Neo-Hookean-like expression fitted before SIC starts provides accurate results and apply both for filled and unfilled NR.*

3. Typical experimental set-ups

A wide range of experimental setups has been developed to characterize the calorimetric response of elastomers, differing in the materials investigated, the applied loading conditions, and the specimen geometries. The aim of this section is to describe how the calorimetric response can be characterized in the simplest way and what are the different families to be distinguished in terms of the calorimetric response. This section is based on tests performed in our group at the Institute of Physics Rennes (University of Rennes, France), which are summarized in Table 1. Only homogeneous strain fields at the macroscopic scale are considered in this section.

3.1. Materials

Several elastomeric materials have been investigated using stretched surface calorimetry. So far, crystallizing NR and Thermoplastic Poly Urethane (TPU), and non-crystallizing Styrene Butadiene Rubber (SBR) and Nitrile Butadiene Rubber (NBR) have been studied. In addition to SIC, other factors affect the calorimetric response, especially the addition of fillers. Fillers induce viscosity and stress softening (the Mullins effect) both of which exhibit distinct calorimetric signatures. Therefore, more than the chemical composition itself, the calorimetric behavior of the elastomers tested can be primarily classified according to four main material families: filled or unfilled, and crystallizing or not crystallizing under strain.

From a thermodynamic point of view, the required material parameters are the density, the thermal conductivity when heat conduction occurs and the heat capacity. Generally,

volume variations are neglected, which simplifies the prediction of $\tau(\lambda)$ (see Section 2.1.1). The heat capacity can be measured as a function of temperature (see for example Ref. 58) or a mean value can be chosen (see for example Ref. 49).

Refs	Material	Filler type and amount (phr)	t x w x l [mm^3]	Loading rate [mm/min]	Strain rate ± [s^{-1}]	Loading conditions	MC	IR camera
[48,83]	NR	0	1.4 x 5 x 10	100, 300	0.167, 0.500	NS, 3 cycles at λ = 2, 5, 6, 7.5	X	CJ
[49]	SBR	5 CB (N347)	1.4 x 5 x 10	300	0.500	NS, 3 cycles at λ = 2, 3, 3.5, 4	X	CJ
	SBR	50 CB (N347)	1.4 x 5 x 10	300	0.500	NS, 3 cycles at λ = 2, 3, 4, 4.5	X	CJ
[50]	NR	50 CB (N347)	1.4 x 5 x 10	300	0.500	NS, 3 cycles at λ = 1.4, 2, 4, 6	X	CJ
	SBR	50 CB (N347)	1.4 x 5 x 10	300	0.500	NS, 3 cycles at λ = 2, 3, 4, 4.5	X	CJ
[52]	SBR	5 CB (N347)	1.4 x 5 x 10	300	0.500	NS, 3 cycles at λ = 2, 3, 3.5, 4	X	CJ
	SBR	50 CB (N347)	1.4 x 5 x 10	300	0.500	NS, 3 cycles at λ = 2, 3, 4, 4.5	X	CJ
	NR	0	1.4 x 5 x 10	300	0.500	NS, 3 cycles at λ = 2, 5, 6, 7.5	X	CJ
	NR	50 CB (N347)	1.4 x 5 x 10	300	0.500	NS, 3 cycles at λ = 1.4, 2, 4, 6	X	CJ
[51][iv]	NR	0	1.4 x 5 x 10	100	0.167	NS, 3 cycles at λ = 2, 5, 6, 7.5	X	CJ
[53]	TPU[v]	0	5 x 9 x 20	100, 300	0.083, 0.250	NS, 5 cycles at λ = 1.5, 2, 2.5, 3	X	FX6
[54]	NBR	0	1.9 x 7.25 x 20	50, 100, 200	0.042, 0.083, 0.167	NS, 5 cycles at λ = 1.5, 2, 2.5, 3, 3.5, 4	X	FX6
	NBR	35 CB (N347)	1.9 x 7.25 x 20	50, 100, 200	0.042, 0.083, 0.167	NS, 5 cycles at λ = 1.5, 2, 2.5, 3, 3.5, 4		FX6

[iv] Experimental data from Refs 47 and 83

[v] Irogan A87H4615 Hunstmann corporation (The Woodlands, Texas)

[55]	NR	0	1.4 x 5 x 10	100	0.167	NS, 3 cycles at λ = 2, 5, 6, 7.5	X	CJ
[56]	NR	0	1.4 x 7.2 x 19.3	100, 200	0.086, 0.173	S, 3 cycles at λ = 7		FX6
[61]	NR	20-30 CB	2 x 10 x 24	300	0.208	S, 3 cycles at λ = 2.5, 4, 6		FX6
[58]	NR	0	2 x [8.36-18.8] x 12	300	0.417	S, 3 cycles at λ = 7		FX6
[57]	NR NR	0 50, 3 CB types	2 x 5 x ca 40[vi] 2 x 5 x ca 40	300 300	ca 0.125 ca 0.125	S, 5 cycles at λ = 6 S, 5 cycles at λ = 2, 3, 4, 5, 6		FX6 FX6

Table 1: Summary of the setups used for surface calorimetry with an IR camera, with t: thickness, w: width, l: length, S: symmetrical tension, NS: non-symmetrical tension, MC: motion compensation of the measurement zone in the IR images, CJ: Cedip Jade III-MWIR 320 x 240 px, FX6: FLIR X6540sc InSb 640 × 512 px, phr: part per hundred of rubber in weight.

3.2. Specimen geometries and loading conditions

Specimen geometries used for uniaxial loadings are thin; 2 mm maximum (to meet conditions exposed in Section 2.1.1), widths between 4 and 20 mm, and lengths of 10 to ca 40 mm. Obviously, the smaller the length, the smaller the width must be to meet uniaxial tension loading condition. The purpose here is not to provide an exhaustive list of the various dimensions reported in the literature, but rather to discuss some experimental precautions. Typically, the initial specimen length has an effect on the measurement: if the loading is applied with only one jaw, the longer the specimen, the greater the displacement in the air of the surfaces to achieve the same stretch, and the more the convection to be forced. This is a key point because τ is evaluated from the thermalization of a static surface. From this point of view, it is preferable to carry out symmetrical tension test whenever possible with the equipment used.[54,56,61] It should be noted that we will not deal with relaxation tests or cyclic tests with relaxation phases, but the reader can refer to Refs 48 and 61 on these subjects. Nor will we discuss tests under heterogeneous loading, which are carried out with 3- or 4-branch specimens and are aimed more at developing methods for motion compensation[60] or inverse identification of constitutive parameters without boundary conditions,[59] or to study the effect of multiaxiality on the calorimetric response[61] or to characterize the functioning of the crack-laying zone.[62-65]

[vi] The specimen ends were wound around a metal axle. The initial length was measured once the specimen was fixed and not buckled.

The loading conditions generally consist of several cycles of increasing strain amplitude. These cycles are also repeated even if the material does not exhibit significant accommodation (stress softening), in order to stabilize the thermal response, which is a key-point for the proper assessment of the intrinsic dissipation.[12] Figure 2 shows a typical loading case, where several cycles (usually 3 to 5 maximum) of increasing maximum strain are applied. The different geometries, loading and thermal measurement conditions are summarized in Table 1.

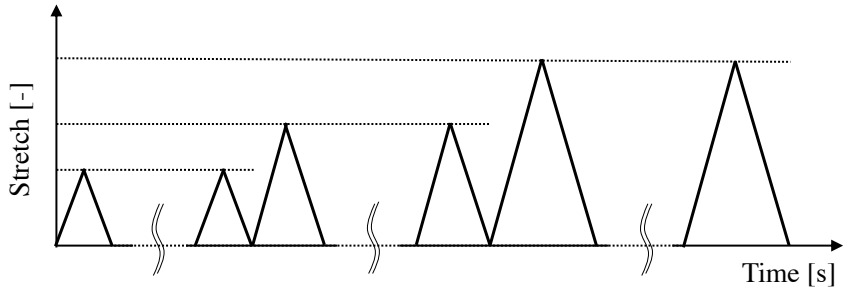

Figure 2: Typical loading profile under uniaxial tension. Several cycles of increasing maximum strain are applied at the same strain rate.

3.3. Temperature measurement

Thermal measurements are performed with IR cameras. The temperature fields obtained allow us to study heterogeneous heat source fields, a typical example being a crack tip zone. The IR cameras are usually turned on several hours before the test to stabilize the temperature of the IR detector matrix. Acquisition frequencies are generally a few tens of Hertz to reduce measurement noise by using filters before deriving temperatures with respect to time. With cooled cameras, the thermal resolution or noise equivalent temperature difference (NETD) is about 20 mK for a temperature range between 5 and 40°C. The spatial resolution of the thermal field ranges generally between 200 and 500 µm/px. The surface emissivity of the tested materials is set at 0.92 ± 0.02. This value was verified with NR specimens, filled and unfilled by comparing the temperature of the specimen surfaces placed in an oven and heated to 50°C with that of a black body regulated at the same temperature. It should be noted that an optical infrared pyrometer could be used for the temperature measurement, especially if the loading is applied symmetrically.

4. Typical results

This section introduces the different types of calorimetric response. They are reviewed from the results reported in Ref. 52. The crystallizable and non-crystallizable rubbers are those among the most produced each year, namely NR and SBR respectively. The filler

type considered was the carbon black, in a quantity of 50 phr. It should be noted that the unfilled SBR was filled with 5 phr to improve its manufacturing. Figure 3 presents their mechanical responses in terms of the nominal stress versus the stretch. The loading was applied under prescribed displacement, at a rate of 300 mm/min (a strain rate of 0.5 s^{-1}).

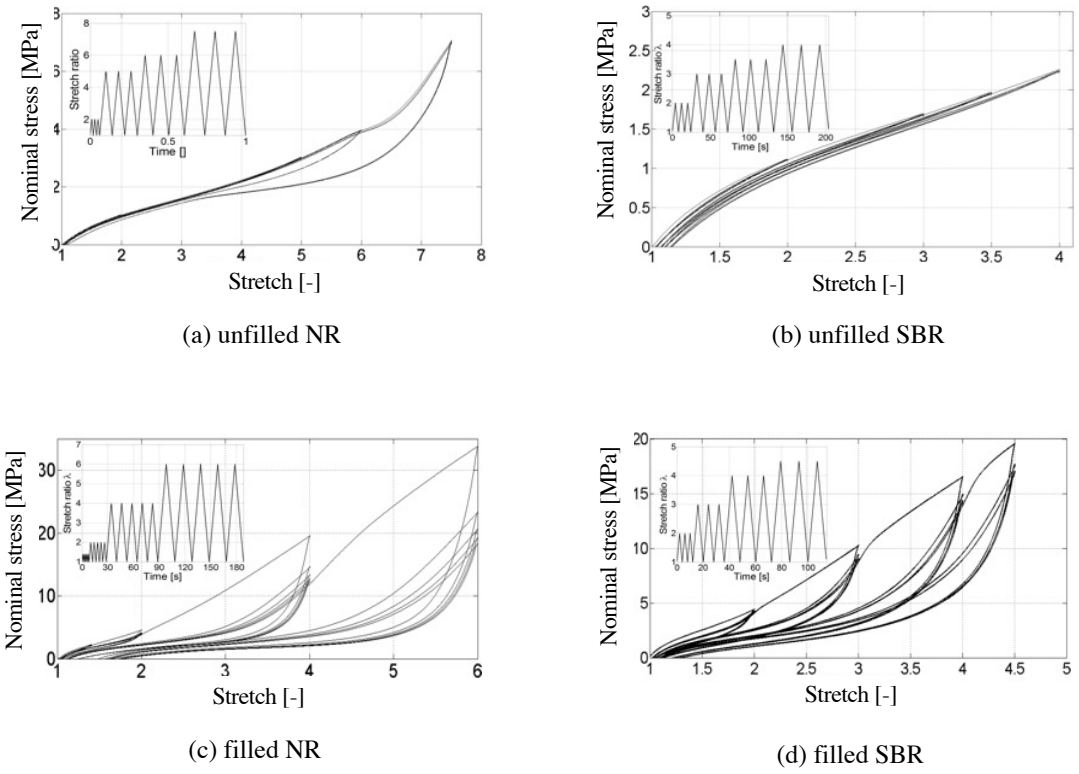

(a) unfilled NR

(b) unfilled SBR

(c) filled NR

(d) filled SBR

Figure 3: Mechanical response of NR and SBR, unfilled and filled with carbon black (from Ref. 52).

For the unfilled rubbers, the mechanical cycles, i.e., the number of cycles at a given stretch, have no effect on the mechanical response. No significant permanent strain was observed in unfilled NR. In SBR, the 5 phr of carbon black may be responsible for the slight residual stretch observed. No hysteresis loop is observed for the SBR. This is also the case with NR if the maximum stretch does not significantly exceed that of the onset of crystallization (approx. 4). For higher stretches, a hysteresis loop is formed. This phenomenon is due to the difference in the kinetics of crystallization and crystallite melting, which was first intuited by Clark as soon as 1940[28] and demonstrated in Refs 48, 51 and 84. As expected, the addition of fillers induces a hysteresis loop (whatever the stretch reached) that decreases with the number of cycles and stabilizes at a given maximum stretch, which is accompanied by a significant permanent stretch and stress softening. These phenomena were first observed by Bouasse and Carrière[19] and extensively studied by Mullins.[21,85,86]

4.1. Calorimetric responses under uniaxial tensile loading

Figure 4 presents the calorimetric responses determined from the temperature measurements and the simplified heat diffusion equation (Eq. (6)).

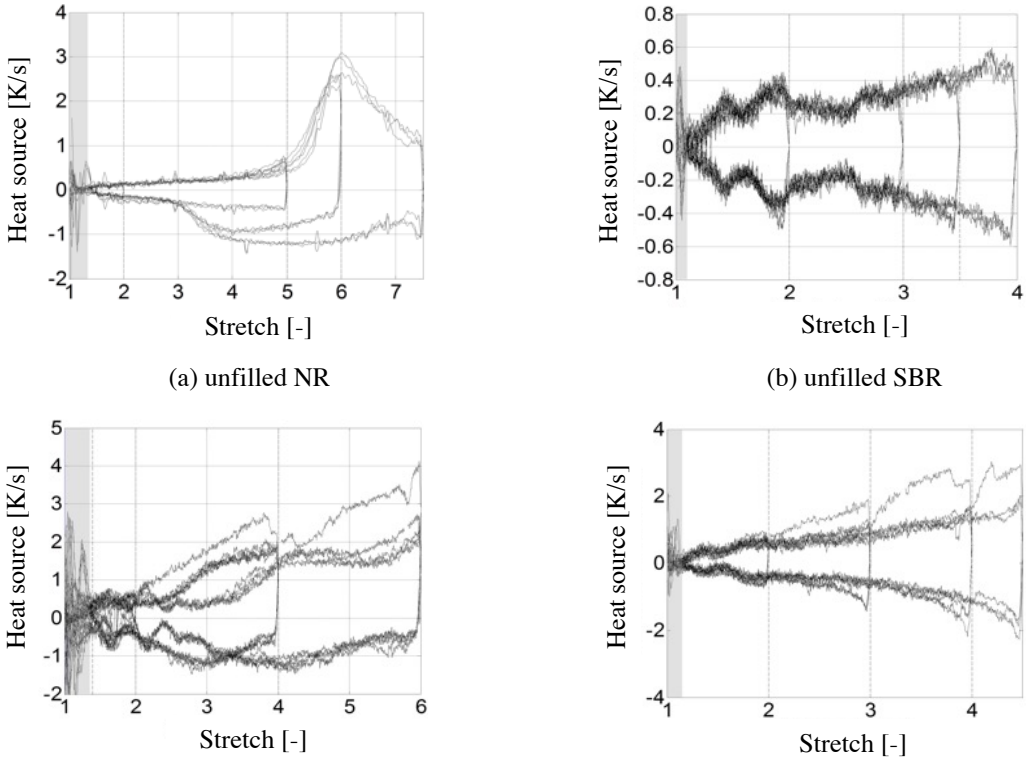

Figure 4: Calorimetric response of NR and SBR, unfilled and filled with carbon black (extracted from data appearing in Ref. 52)

In the literature, the calorimetric response is given either in W/m^3, the unit of $\hat{S}$, or in K/s, the unit of $\frac{\hat{S}}{\rho_0 C}$. This latter unit has a more intuitive meaning, i.e., the amount of Kelvin gained or lost per unit of time. For all the compounds, an increase in the stretch induces an increase in the heat source. This is a consequence of the entropic elasticity, which is preponderant in rubbers compared to non-entropic (energetic) elasticity. It should be noted that for the lowest stretches, a thermoelastic inversion is generally observed, which corresponds to an inversion in the heat source sign. This is not discussed in this chapter, but the reader can refer to Refs 47, 83 and 87 for further information on this phenomenon that is due to non-entropic effects.

In filled NR, the stabilized heat source is close to the maximum heat source obtained in unfilled NR at a given maximum stretch, which was not the case for SBR. In fact, at $\lambda = 4$, the heat source in filled SBR is approximately 4 times that in unfilled SBR. A strong

difference (a factor 3 at $\lambda = 4$) was also observed with a non-crystallizing NBR in Loukil et al[54], unfilled and filled with 35 phr of carbon black. This difference was shown not being affected by the loading rates that were applied (see the loading rate range in Table 1). It should be noted that for the unfilled and the stabilized response of filled SBR, the heat source is symmetrical between the loading and unloading. For the unfilled NR, it is observed when the maximum stretch applied is inferior to λ_C. For the filled NR, λ_C is much smaller and further investigations should be carried out to discuss any symmetry of the stabilized cycle when no SIC occurs during the cycle. In the next paragraphs, special attention is paid on the calorimetric signature of the different phenomena involved in the rubber deformation.

4.2. Heat sources due to SIC

4.2.1. Qualitative analysis on how SIC and crystallites melting affect the calorimetric response

The effects of SIC and crystallite melting on the calorimetric response can be discussed by testing an unfilled NR, which hysteresis loop is due neither to viscosity nor stress softening. Fig. 4(a) highlights indeed strong singularities in the calorimetric response of unfilled NR compared to the unfilled non-crystallizing SBR (see Fig. 4(b)). As the stretch rate is constant over the test, these singularities can only be due to strain-induced crystallization and crystallite melting. When the mechanical cycles are performed at maximum stretches inferior to λ_C, the heat source evolves symmetrically between loading and unloading with respect to the zero heat source axis. This indicates that no intrinsic dissipation has occurred. The symmetry is lost when a maximum stretch equal to 5 are applied. During loading, the heat source evolves quasi-linearly until reaching a stretch close to λ_C, from which an exothermal peak forms. Moreover, Samaca Martinez et al[48] found that the areas under the loading and unloadings curves were equal, which confirms that no heat was produced due to intrinsic dissipation for the loading conditions tested. When the maximum applied stretch increases, loading-unloading dissymmetry increases as the maximum crystallinity reached increases. From a mechanical point of view, the area of the hysteresis loop also increased with the maximum stretch reached. As no mechanical dissipation was detected, this is the demonstration that a hysteresis loop can form without any detectable intrinsic dissipation and can only be due to thermomechanical coupling due to SIC. From stretches equal to 6 during the loading phase, the heat source decreased instead of increasing continuously. As the heat source remains positive, this means that heat continues to be produced, but at a lower rate. Several causes were addressed in Le Cam et al:[51] (i) the crystallinity saturation if any is approached; (ii) the contribution of internal energy increases due to crystallite deformation; (iii) a less exothermal crystallization process for the highest stretches.

4.2.2. Quantitative analysis: determination of the crystallinity from the calorimetric response

As the crystallization is strongly exothermal and a link is established between the crystallinity and the fusion enthalpy, the density, the heat capacity, the temperature variation due to SIC, the crystallinity can be measured from the calorimetric response by applying the method described in Section 2.3.

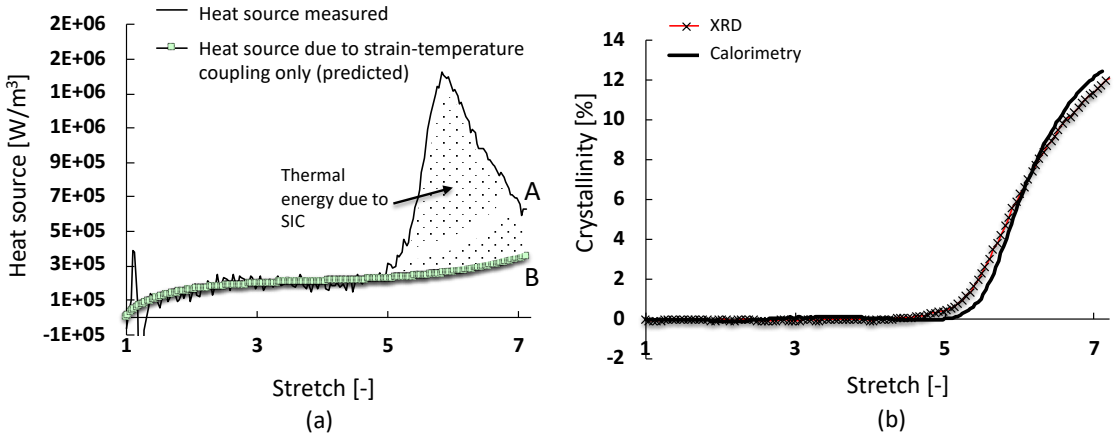

Figure 5: (a) Heat sources measured (curve A) and predicted (due to strain-temperature coupling, curve B) during the loading: (cycle stabilized thermally, loading rate of 200 mm/min) (b) Comparison between calorimetry-based and XRD-based crystallinity measurement

First of all, Fig. 5(a) shows the variations of the heat source measured during the test (curve A), as well as a prediction of the heat source without crystallization (curve B) for an unfilled NR different from those in the previous sections (information on the material is given in Le Cam et al[56]). This prediction is made using the method described in Ref. 55. The area between curves A and B corresponds to the thermal energy of crystallization. This energy is used to derive the crystallinity. The result obtained is compared with the XRD measurement in Fig. 5(b). This figure shows the surface calorimetry technique provides an accurate crystallinity measurement. The results obtained by Le Cam et al[57] show that the tangent or the Neo-Hookean-like prediction used to fit the heat source before SIC starts provide an accurate measurement of the crystallinity.

4.3. Heat sources due to viscosity and stress softening in filled rubbers: determination of the mean intrinsic dissipation

When fillers are added to the compounds, the first mechanical cycle at a given maximum stretch ratio exhibits a higher maximum heat source and a decreasing value until

stabilization for the following cycles. All the cycles, even the first one, show the same heat source evolution during the unloading. This is clearly shown in Figs. 4(c) and (d). Therefore, the calculation of the mean intrinsic dissipation $\widetilde{\mathcal{D}}_{int}$ applied to the first cycle provides an evaluation of the mean intrinsic dissipation due to the stress softening and to the viscosity. The calculation applied to the stabilized (mechanical and thermal) cycles provides the mean intrinsic dissipation due to viscosity.[vii]

Thus, the mean intrinsic dissipation due to viscosity can be removed from the mean intrinsic dissipation of the first cycles in order to evaluate the mean intrinsic dissipation due to the stress softening. Figure 6 gives an example of the mean intrinsic dissipation due to Mullins effect and to viscosity in the filled NR tested in Khiem et al[61]. It is observed that $\widetilde{\mathcal{D}}_{int}$ is almost linear with stretch for the applied loading conditions. This is an important information for modeling the viscosity and the Mullins effect in filled rubbers.

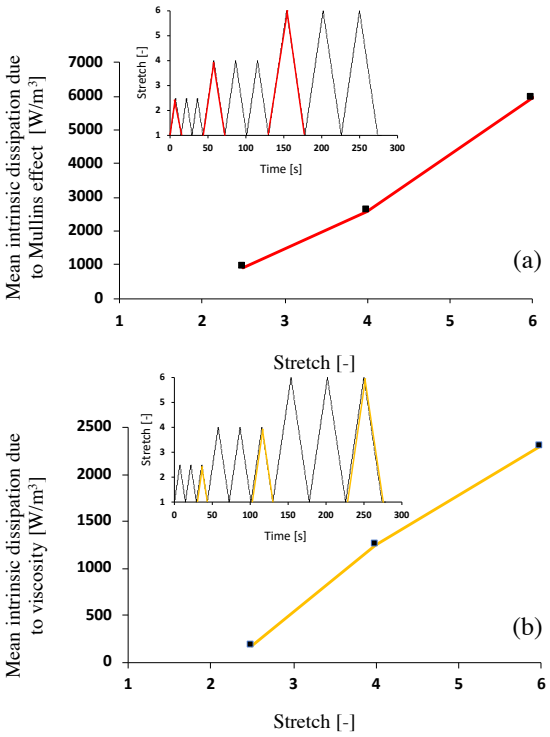

Figure 6: Mean intrinsic dissipation ($\widetilde{\mathcal{D}}_{int}$) versus stretch due to (a) the Mullins effect and (b) the viscosity. The lines are guides to the eye.

[vii] The mean intrinsic dissipation has to be calculated over a thermodynamic cycle, i.e., with the same temperature and strain between the loading beginning and the unloading end[12]. This means that only the mechanical and thermally stabilized cycle provides quantitative data on the heat source produced by the viscosity.

4.4. Investigating how rubbers use the mechanical energy to deform: an energetic approach

The previous results clearly demonstrate that the mechanical energy involved in the hysteresis loop is not systematically dissipated into heat, the typical example being the hysteresis loop observed in the mechanical response of unfilled NR only when SIC occurs. The fact that the hysteresis can be partly or even not be due to viscosity explains why it cannot be time-dependent[54,86-91] and why the self-heating under repeated cycles is much less than the one predicted by assuming that all the energy involved in the hysteresis loop is converted into heat. This is generally observed by measuring the self-heating during fatigue-like test loadings.[92-94] Thus, other factors contribute ot the mechanical hysteresis:

(a) The thermal dissipation (under non-adiabatic test conditions). In most of the homogeneous (in terms of heat source field) tests performed, considering the thermal properties of elastomers and the loading rate relatively high, the thermal dissipation does not contribute significantly to the mechanical hysteresis;

(b) The changes in microstructure modeled by thermomechanical couplings. In this case, as observed by Mott et al[95] for polyurea, all the work done to the system is not measured as an apparent temperature change. The authors concluded that a significant part of the mechanical energy is used by the material to reorganize, which changes its internal energy. The authors also related this mechanical energy "lost" in the microstructure to the residual strain. This result could be discussed in terms of energy stored and not released. Le Cam[51] showed that the mechanical hysteresis of the unfilled NR he studied was entirely due to the difference in kinetics between crystallization and crystallite melting. No residual strain accompanied the occurrence of the hysteresis loop. Therefore, energy is stored in the material during the crystallization process and is released at a different rate during melting. This energy storage may be due not only to the SIC, but also to the filler network. In fact, Loukil et al[54] demonstrated that filled NBR he studied stored part of the mechanical energy in the filler network reorganization and released it at a different rate during unloading. This should be due to the fact that the viscous effect due to fillers change the kinetics of energy storage and release between loading and unloading.

Therefore, the amount of self-heating, or more relevantly, the mean intrinsic dissipation, must be put into perspective in relation to the energy rate involved in the hysteresis loop. Even more interesting is the part of the mechanical energy brought that is stored and released by reversible microstructure changes and is not dissipated as heat or used to damage the material, for example to propagate cracks. This is the aim of the stored energy ratio γ_{se} defined in Section 2.3, which enables us to characterize and to compare elastomers according to their energetic behavior. An illustration is given in Figure 7 for 3 different materials. The data are available in Lachhab et al[53] for the TPU, in Loukil et al[54] for the filled NBR and in Samaca Martinez et al[48] for the unfilled NR. Only the zones containing the responses are represented here. It is shown that the energetic response of

unfilled NR does not depend on the stretch, nor on the stretch rate (in the range investigated). Similar to unfilled NR, TPU response is not stretch-dependent. Nevertheless, it depends on the stretch rate and on the density but the responses are included in a range where γ_{se} is close to one. These similarities in terms of energetic behavior echo those in terms of crack growth resistance. For the filled NBR, γ_{se} depends on both stretch and stretch rate. This type of energetic map brings new insights for understanding how rubbers use the mechanical energy to deform and motivate the systematic measurement of the temperature during mechanical test. The use of such an approach in order to accelerate the durability prediction of elastomers is discussed in Ref. 84.

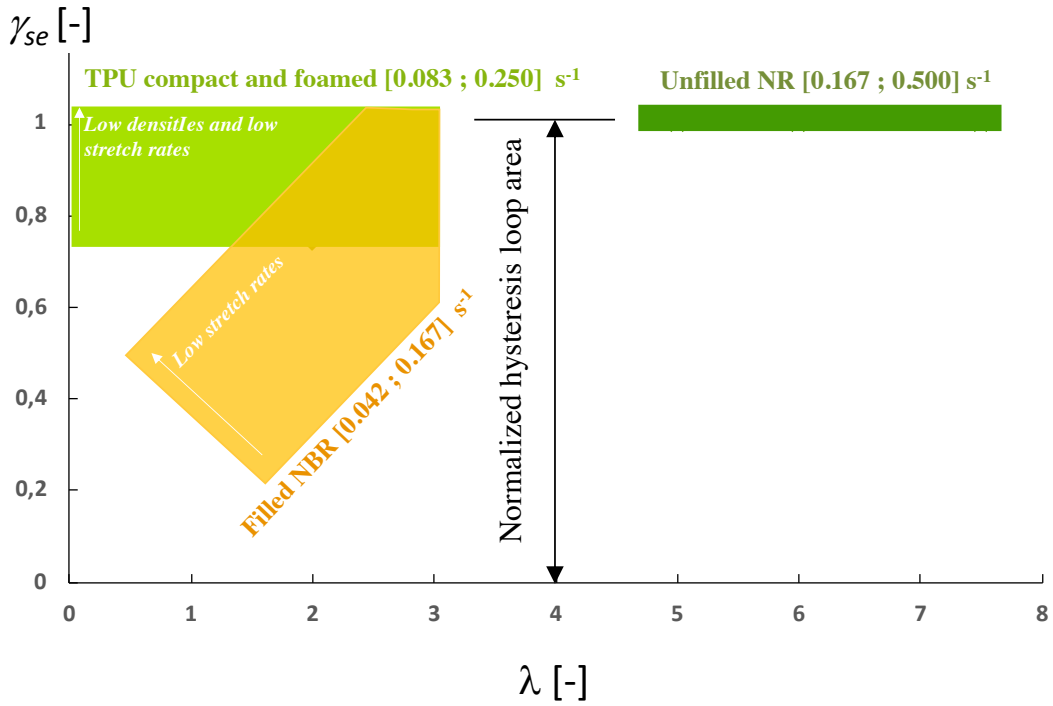

Figure 7: γ_{se} evaluated from thermodynamic cycles for 3 types of elastomeric materials.

5. Heterogeneous heat source fields

There are many reasons to take an interest in heterogeneous heat source fields, whatever they are due to material-related or geometry-related heterogeneities. This section aims at illustrating some of the numerous situations that can be encountered.

5.1. Heterogeneity due to heterogeneous crystallization under homogeneous loading

In our group, we regularly observed heterogeneous temperature fields with cruciform specimens made of unfilled natural rubber in areas where the mechanical field is assumed to be quasi-homogeneous (uniaxial tension). The kinematic measurements carried out highlighted that the local maximum principal stretches reached in these areas is superior to the SIC onset. Fig. 8(a) illustrates the phenomenon observed, and highlights that the hottest zones during loading were the coldest ones during unloading. We decided to investigate this heterogeneity using homogeneous uniaxial tensile tests and surface calorimetry. The study is fully detailed in Ref. 58. The results are summarized in Figs. 8(b) to (d). Fig. 8(b) shows that highly heterogeneous thermal fields take place once the SIC onset (a stretch equal to ca 4) is exceeded, the thermal field being homogeneous below this value. Fig. 8(c) highlights that thermal gradients take place at the same location between cycles #2 and #3, for two different sulphur amounts, which seems to indicate that they are rather due to material heterogeneity than to thermomechanical test conditions. Moreover, preliminary tests enabled us to check that the emissivity field does not become heterogeneous when increasing the stretch. Such heterogeneity is not detected in the strain field as SIC is strongly exothermal but initiates at a very local scale compared to the spatial resolution of the kinematic field measured with the DIC technique. A surface calorimetry analysis enabled us to evaluate the crystallinity along the width at half-height of the specimen. As the loading was applied symmetrically, the displacement of the material points at the specimen's surface was tracked only along its width. Fig. 8(d) gives the crystallinity profile obtained in the case of NR vulcanised with 1.2 phr of sulphur. A difference of ca 3% is observed between the maximum and minimum crystallinity. Differences of the same order of magnitude was also observed for other sulphur amounts and geometries (more less large) in Ref. 58. This was the first evidence of SIC heterogeneity under a homogeneous loading, which could be explained by strain/stress concentrations at the macromolecular scale that initiate SIC: (i) the distribution in the active chain density (ii) the presence of particles. These results obtained by surface calorimetry are of interest in that they provide access instantly to several continuum quantities, especially state variables, which is of primary importance to enrich and validate constitutive models (see for instance Ref. 96). This is not the case with other methods. Furthermore, these results show that it is necessary to consider several spot measurements on the same specimen for rigorously determining the average crystallinity during deformation.

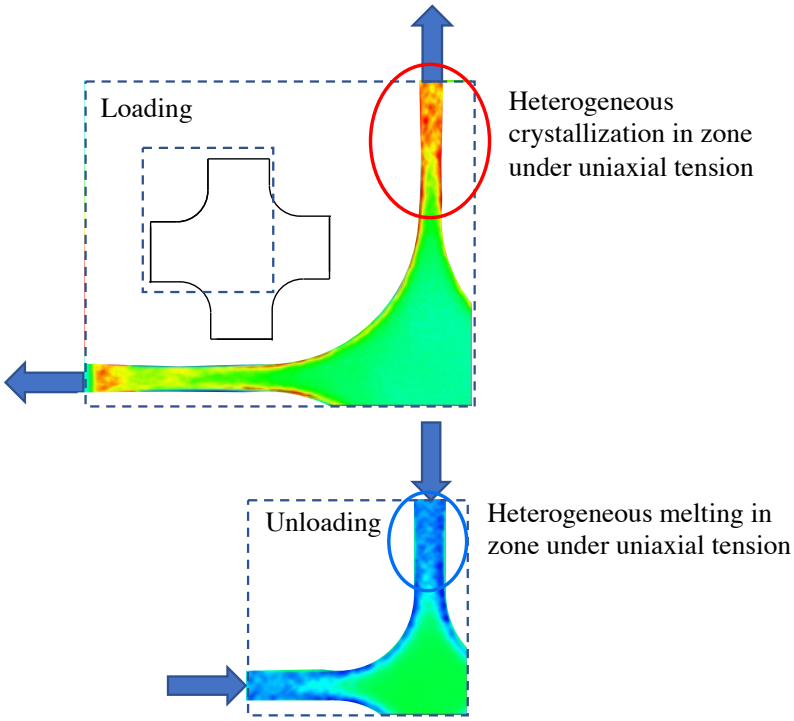

(a) Equibiaxial tensile test

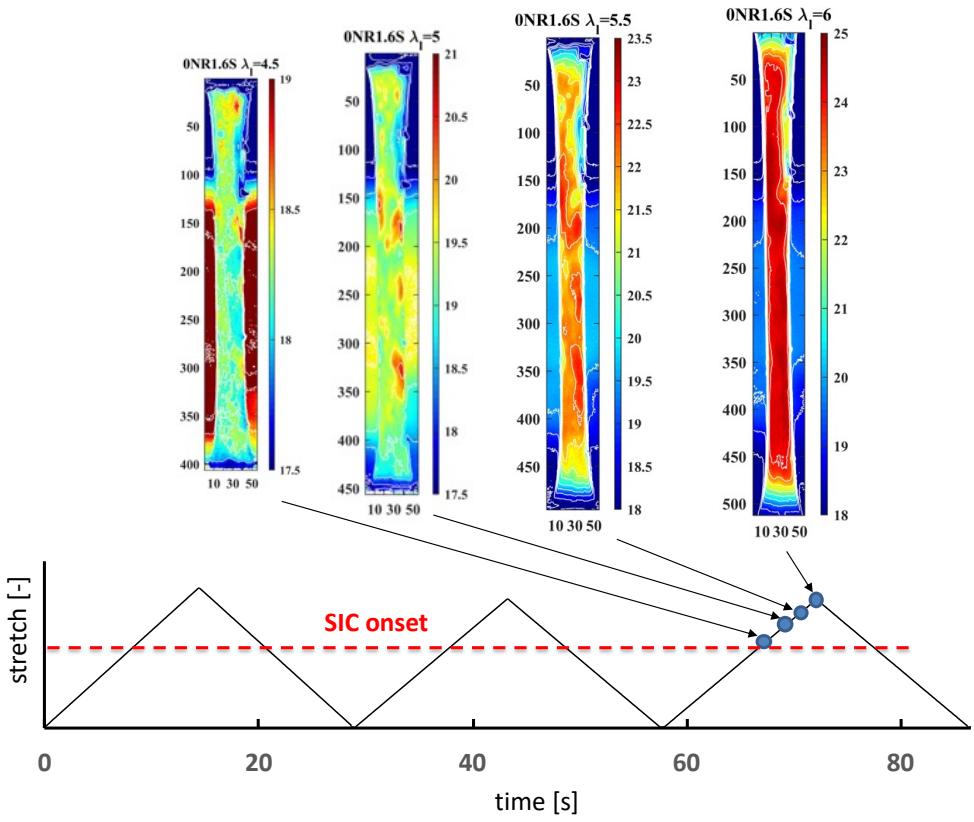

(b) Uniaxial loading conditions. Thermal fields stored during the third cycle for stretches superior to the crystallization onset.

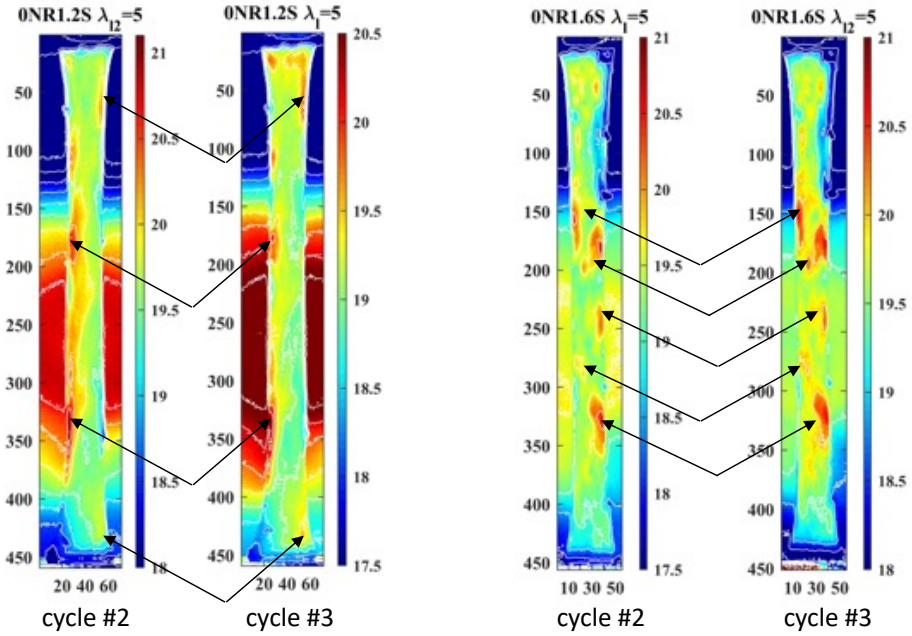

(c) Comparison of the heterogeneity in the thermal field at a stretch equal to 5 between the loading of cycles #2 and #3.

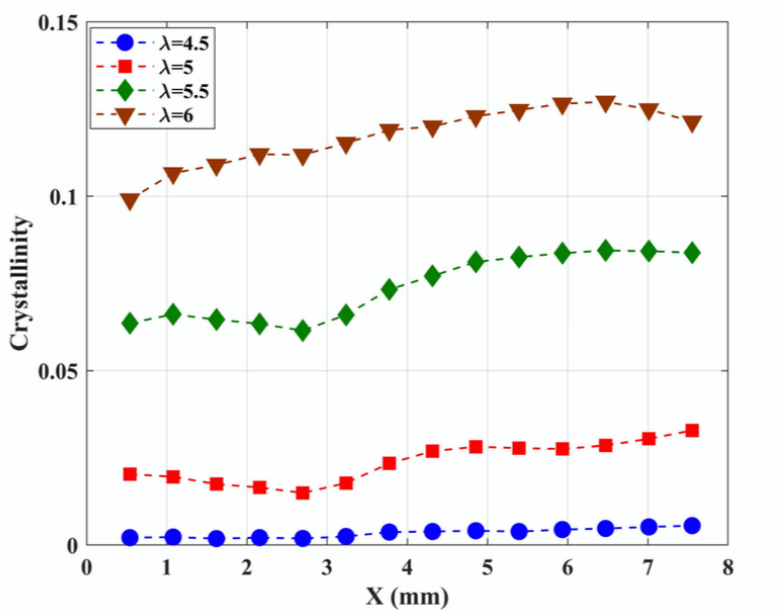

(d) Crystallinity profile for NR vulcanized with 1.2 phr of sulphur. The loading is applied symmetrically and the displacement of the points at the specimen mid-height are tracked along the width with a geometric transformation.

Figure 8: Heterogeneous crystallization under uniaxial tension.

5.2. Inverse identification of constitutive parameters

As many models do not account for the numerous phenomena involved in the deformation process, the values of the constitutive parameters strongly depend on the strain state. [97] This is the reason why constitutive parameters of hyperelastic models are classically identified from several homogeneous tests, namely the uniaxial tensile (UT), the pure shear (PS) and the equibiaxial tensile (EQT) or uniaxial compression (UC). These three tests completely described the domain of possible loading paths.[38, 97, 98, 99] A trade-off between the sets of values obtained with the different tests has therefore to be found to obtain parameters that can reasonably be considered as intrinsic to the mechanical behavior of the material. Such identification approach has several disadvantages: (i) each of the tests carried out are assumed to induce a homogeneous strain state, which is a strong assumption in case of PS and EQT tests (ii) several specimen geometries, i.e. molds, are required (iii) several testing machines are needed to apply these loading conditions (iv) dispersion obtained for each test requires testing several specimens for each loading condition (v) the comparison between the constitutive parameters identified from different loadings is a matter of debate. For instance, should the identification be made for a same maximum stretch applied, the same energy, etc? (vi) the elaboration process may differ from one specimen geometry to another one (typically compression molding versus injection molding). This can have a significant effect on the value of the identified constitutive parameters.

Since the end of the 2000s, alternative approaches have been proposed. They are based on heterogeneous tests that induce the three strain states mentioned above and a wide range of intermediary strain states.[99, 100, 101, 102] In these approaches, the boundary conditions (force and displacement) are required to solve the identification problem as well as the kinematic field (see Refs 101 and 102 for the Virtual Field Method (VFM) and Refs 103 and 104 for the Finite Element Model Updating (FEMU)). This section illustrates the perspective offered by coupling full kinematic and thermal field measurements for identifying constitutive parameters at the local scale, without measuring boundary conditions.

Considering that the heat sources can be obtained from two different ways; the temperature field processed with the heat diffusion equation and the kinematics field coupled with a constitutive thermomechanical model, the constitutive parameters of the thermomechanical model are the only unknowns that can therefore be identified. Thus, at any point of the surface observed, the constitutive parameters can be identified without using the boundary conditions. This idea has been explored in Ref. 59, where a cruciform-shaped specimen is stretched under equibiaxal tension. The heat source field is determined by applying the bidimensional formulation of the heat diffusion equation (Eq. (4)) to the temperature field measurement. A motion compensation of point in the IR images requires a kinematic field measurement. In the case of the large deformations of rubber, the Digital Image Correlation (DIC) technique is generally used. Different methods have been developed for compensating large displacements of points in the IR

images, the reader can refer to Refs 59 and 60 for further information. It should be noted that if the Eulerian formulation of the heat diffusion equation is chosen, the Laplacian operator appears in the equation in the case of isotropic conductivity, and the speed of the material points has to be calculated. The calculation has to be done for each intermediary loading state. The reference image must be pushed forward in each intermediary configuration to obtain the temperature changes to be processed. In the Lagrangian description, which is the one chosen in this study, the speed of the points is zero, but the calculation of the heat influx per unit reference area is more complicated (see Eq. (3)). Moreover, the thermal field has to be pushed back to the reference configuration for the spatial derivative. If the diffusion length is small enough compared to the spatial resolution of the thermal measurement, the heat conduction can be neglected and the "0D"-like formulation of the heat diffusion equation can be used at any point of the field. The heat source field reconstruction requires the preliminary characterization of τ_{2D} according to the stretch and the biaxiality coefficient. The accurate evaluation of this parameter is all the more important that the test is performed at a low loading rate, leading to significant heat exchange by convection and low temperature variations. In this study, an unfilled Nitrile Butadiene Rubber (non-crystallizing and not viscous) has been chosen. Figure 9 presents the surface obtained by plotting τ_{2D} from the measurement of τ_0 in the undeformed state.[viii] The black crosses correspond to a measurement performed at the maximum displacement applied to the four specimen's branches (70 mm prescribed to each branch). This figure highlights the good estimation of τ_{2D} by Eq (5), which avoids characterizing at different stretch levels as well as SIC effects when the material is crystallizable.

[viii] *It should be noted that a halo may form whatever the result of the Non-Uniformity Correction (NUC) of the IR detector matrix. Therefore, the temperature fields are 'altered' by an additional non-uniform temperature distribution due to a halo, which amplitude is about a few tenths of a degree (see Ref. 62). This halo has to be characterized and if significant, has to be removed from the temperature maps before applying the heat diffusion equation if the points observed move through it. A special attention must be paid on the consequence of the configuration chosen (Eulerian or Lagrangian) for removing the halo.*

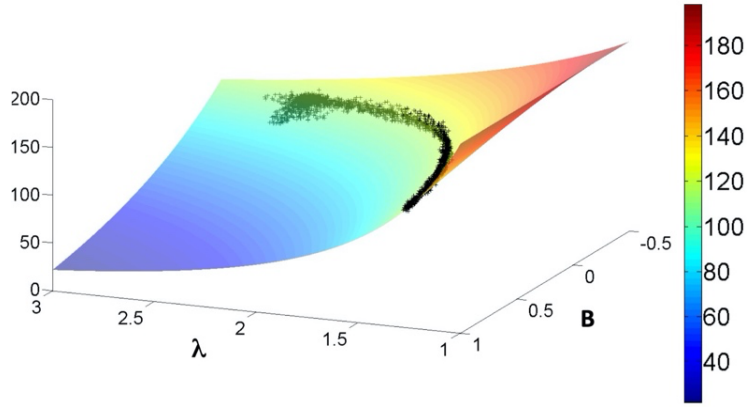

Figure 9: τ_{2D} (in s) versus the stretch and the biaxiality coefficient B. (from Ref. 59). Black crosses correspond to the measurements.

In this study, the Neo-Hookean model is used. It writes with only one parameter. Figure 10 illustrates well that this parameter is strongly affected by the loading state, in particular between the equibiaxial tension (on the left-hand side, toward the specimen centre) and the two other types of loading; uniaxial tension in the branch and pure shear in between. This is explained by fact that the mechanical response of rubber-like materials is governed by numerous phenomena that are not taken into account by the model chosen. Such an approach is therefore as much useful for the identification as for detecting model limitations.

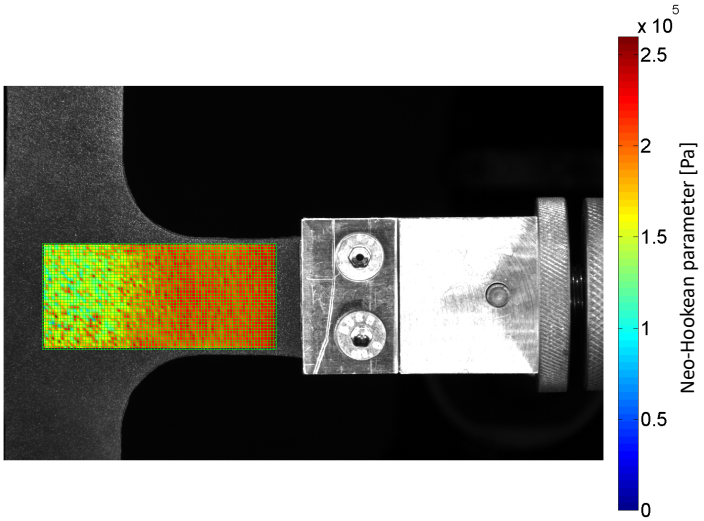

Figure 10: Neo-Hookean parameter field in the undeformed state or the maximum displacement applied (from Ref. 59).

5.3. Thermomechanical and calorimetric characterization of crack tip zones

Similarly to the previous case, heterogeneous heat source fields induced in the vicinity of a crack tip have to be reconstructed by coupling imaging systems in the visible and infrared domains to track the points that are moving in the IR images. Contrarily to the previous case, gradients in the strain and thermal fields are much stronger and require revisiting movement compensation technique and heat source reconstruction methods whose metrological performances have to be fully characterized and drastically improved. Owing to the wide range of cameras suitable for this application, as well as to the testing machines whose capabilities may differ from one laboratory to another, the present analysis was conducted for a given setup. It is precisely detailed in Ref. 105. Consequently, the results reported herein are strictly valid only for this specific set of equipments and mechanical testing configuration.

Regarding motion compensation, thermal measurements were carried out on a cardboard plate subjected to translational motion. An illustration is provided in Figure 11. The surface corrugations give rise to apparent emissivity variations, resulting in temperature fluctuations of several tenths of a Kelvin. This magnitude is one order of magnitude more than the thermal resolution of the infrared camera used.

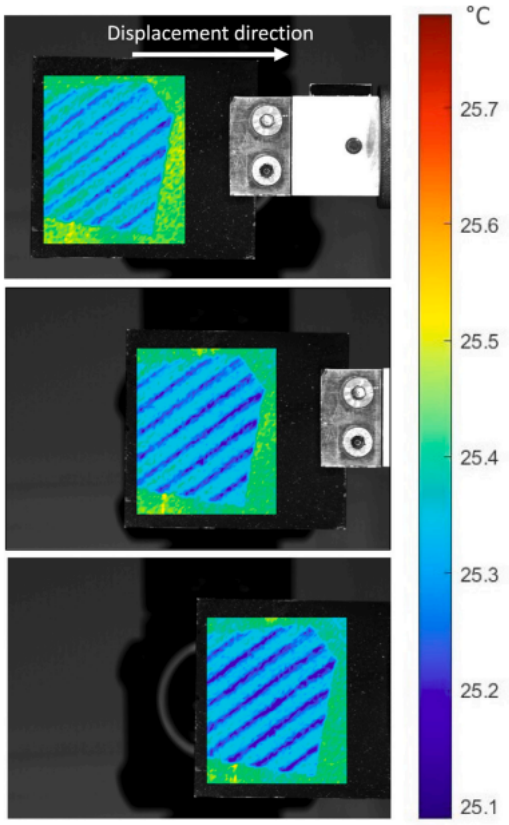

Figure 11: IR images of the corrugated cardboard plotted at different positions in the visible images (from Ref. 105). The cardboard was glued on a metallic plate painted in black color.

The variations in a wide range of parameters have been considered: the loading rate, the acquisition frequency, the distance between the IR detector and the specimen as well as the distance between the CCD detector and the specimen. The influence of the step size, the subset size and the interpolation function was also investigated for the DIC technique, as well as the temporal filtering of the temperature variations. The different test configurations are precisely described in Ref. 105. They have been chosen accordingly to the features and limitations of the experimental setup used. In order to evaluate the thermal resolution, the standard deviation of the temperature variation signal has been calculated at any point of the field during a return trip in translation. The mean of the standard deviation field has then been calculated for each configuration and the performance of the method has been evaluated by measuring the standard deviation of the temperature of each material point and compared with the Noise Equivalent Temperature Deviation (NETD of 20 mK) of the IR camera. It was found that that the compensation technique does not alter the thermal resolution in the variation range of experimental parameters in relation with the experimental setup used. Regarding heat source reconstruction, the determination of the resolution is not detailed here, but it is fully explained in Ref. 105. The heat source resolution reached is less than $5\ 10^3$ W/m^3, which is two orders of magnitude less than the heat source values classically measured for stretched elastomers.

The methodology has been applied to a stretched crack tip in an unfilled natural rubber specimen. The crack tip was observed after several hundred of mechanical cycles applied to the notched specimen. The quantitative analysis of the different fields and profiles plotted (along the crack lips and behind the crack tip) enabled us to characterize and to compare the different gradients in terms of strain, temperature, heat source and crystallinity at the same global stretch. This is illustrated in Figure 12. The movies are all downloadable on the Medeley Data web site. The links are provided in Refs 106 to 109.

Quantitative analysis of the results provided in Ref. 65 supports the assumption that under the conditions of the experiment, the crack tip is the most stretched zone but not the most crystallized one, compared to the zones on both sides of it. The results also suggest that cavitation and/or decohesion might locally occur at the crack tip and frustrate the crystallization, which is in a very good agreement with recent results obtained by using the XRD technique.[110]

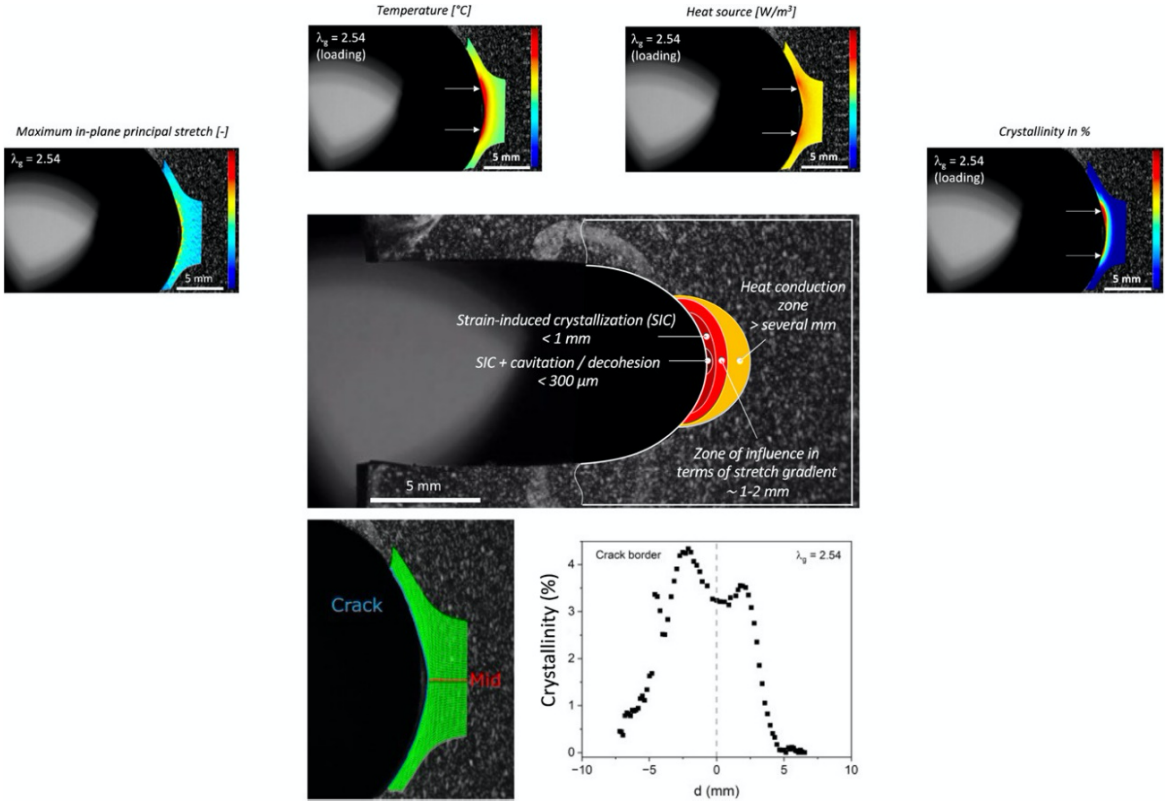

Figure 12: Full strain, temperature, heat source and crystallinity fields at the same global stretched crack tip in an unfilled natural rubber specimen. The crack tip was observed after several hundred of mechanical cycles applied to the notched specimen. Illustration (bottom right) of the crystallinity profile along the crack border (from Ref. 65).

6. Conclusion

This document aims to provide the basics of the calorimetric approach using infrared thermography to study the thermomechanical and energy behavior of materials undergoing large deformations. It reviews the calorimetric signatures of the main phenomena involved in the rubber deformation, i.e., entropic and energetic elasticity, reinforcement by fillers, strain-induced crystallization, stress softening and energy storage. It is fully inspired from Refs 105 and 111 (Chapter 1). The possibilities offered for studying heterogeneous heat source fields were also presented in various scenarios, namely material-related and geometry-related heterogeneities.

The main conclusions can be summarized as follows:

- when the rubber is stretched (relaxed), entropic elasticity is the major contributor to the calorimetric response and leads to heat production (absorption). The load-unload heat source curves are symmetrical in an unfilled and non-crystallizing rubber. This does not mean that the material behaves systematically as a pure entropic material, for which the strain power density and the heat power density superimpose, see for

instance Ref. 51 where the effect of changes in the internal energy on the calorimetric response in a given natural rubber is investigated,

- the symmetry in the heat source between loading and unloading in unfilled NR is no longer observed if crystallization starts. The areas under the calorimetric load-unload curves are equal, meaning that crystallization and melting occur without detectable intrinsic dissipation,
- addition of fillers induces viscosity and stress softening, which is accompanied by the production of intrinsic dissipation that can be quantified and related to the energy rate of the mechanical hysteresis with the γ_{se} ratio,
- the mechanical and the calorimetric responses do not systematically stabilize at the same number of cycles. This has to be taken into account since the mean intrinsic dissipation must be determined from a thermodynamic cycle. In other terms, the mean intrinsic dissipation due to the Mullins effect cannot be rigorously determined, only evaluated, from this technique,
- constitutive parameters of thermomechanical models can be identified at the local scale solely through the coupling of imaging techniques, without relying on boundary conditions. This approach opens the way to improved validation and identification of models aimed at predicting stress and temperature fields in regions exhibiting strong singularities, such as crack-tip zones,
- the crystallinity in unfilled NR was found to be heterogeneous at the macroscopic scale. Differences in the order of magnitude of one percent can be found from one point to another at the surface of a stretched specimen,
- the analysis of kinematic and thermal fields acquired simultaneously and processed to obtain heat source and crystallinity fields provides first-order information on the thermomechanical behavior. The level of technical maturity reached in recent years within our group now makes it possible to achieve spatial, thermal, and calorimetric resolutions compatible with measurements at crack tips.

In conclusion, surface calorimetry offers a wide range of complementary information to better understand the deformation and damage mechanisms in rubbers. The perspectives offered by the extension of this technique to heterogeneous heat source fields are significant, typically to identify constitutive parameters, to characterize heterogeneities in the strain-induced crystallization process, or to study the calorimetric behavior of the crack tip zone in crystallizing rubbers.

The ability to simultaneously obtain continuum quantities, in particular state variables, makes it possible to enrich and validate thermomechanical behavior models (see for instance Ref. 96). Although large deformations complicate the implementation of the technique and require significant development efforts within laboratories, there is growing interest in its use, as illustrated by the recent studies reported in Refs 112 to 114.

7. Acknowledgments

The research activities conducted at the Institute of Physics Rennes have benefited from extensive support, both in terms of financial resources and through rich scientific exchanges. All contributors are gratefully acknowledged:
- the Association nationale de la recherche et de la technologie (ANRT) for the financial support (CIFRE grant) of the PhD theses of Dr. Samaca Martinez and Dr. Lachhab, and the "Programme doctoral normalien.nes" from Ecole Normale Supérieure de Rennes (CDSN grant) for the PhD thesis of Dr. Charlès, Région Bretagne, Rennes Métropole, the Département d'Ille et Vilaine and the European Union (CPER-FEDER 2015–2023 "Institut du Verre"),
- the companies PCM (France), Cooper Standard (France), Continental (France), La Manufacture des Pneumatiques Michelin (France),
- Dr. Robin, Dr. Miroir, Mr. Le Fur and Mr. Burgaud, from the University of Rennes (France), Prof. Balandraud from Sigma Clermont (France), Prof. Toussaint and Prof. Grédiac from the University Clermont-Auvergne (France), Prof. Itskov and Dr. Khiem from the University of Aachen (Germany).

8. References

1. W. S. Farren and G. I. Taylor. The heat developed during plastic extension of metals. Proceedings of the Royal Society of London A: Mathematical, Physical and Engineering Sciences, 107(743):422–451, 1925.
2. G. I. Taylor and H. Quinney. The latent energy remaining in a metal after cold working. Proceedings of the Royal Society of London A: Mathematical, Physical and Engineering Sciences, 143(849):307–326, 1934.
3. A. Chrysochoos. Energy balance for elastic plastic deformation at finite strain (in french). Journal de Mécanique Appliquée, 5:589–614, 1985.
4. A. Chrysochoos, O. Maisonneuve, G. Martin, H. Caumon, and J. O. Chezeau. Plastic and dissipated work and stored energy. Nuclear Engineering and Design, 114:323–333, 1989.
5. J.J. Mason, A.J. Rosakis, and G. Ravichandran. On the strain and strain rate dependence of the fraction of plastic work converted to heat: an experimental study using high speed infrared detectors and the Kolsky bar. Mechanics of Materials, 17(2):135 – 145, 1994.
6. D. Rittel. On the conversion of plastic work to heat during high strain rate deformation of glassy polymers. Mechanics of Materials, 31(2):131 – 139, 1999.
7. W. Oliferuk, M. Maj, and B. Raniecki. Experimental analysis of energy storage rate components during tensile deformation of polycrystals. Materials Science and Engineering: A, 374(1):77 – 81, 2004.
8. M.B. Bever, D.L. Holt, and A.L. Titchener. The stored energy of cold work. Progress in Materials Science, 17:5–177, 1973.
9. A. Chrysochoos and H. Louche. Thermal and dissipative effects accompanying Lüders band propagation. Mat Sci Eng A-struct, 307:15–22, 2001.

10. B. Berthel, B. Wattrisse, A. Chrysochoos, and A. Galtier. Thermoelastic analysis of fatigue dissipation properties of steel sheets. Strain, 43:273–279, 2007.
11. B. Wattrisse, A. Chrysochoos, J.-M. Muracciole and M. Nèmoz Gaillard. Analysis of strain localization during tensile tests by digital image correlation. Experimental Mechanics, 41:29–39, 2001.
12. A. Chrysochoos, V. Huon, F. Jourdan, J.-M. Muracciole, R. Peyroux, and B. Wattrisse. Use of full-field digital image correlation and infrared thermography measurements for the thermomechanical analysis of material behaviour. Strain, 46:117–130, 2010.
13. D. Rittel and Y. Rabin. An investigation of the heat generated during cyclic loading of two glassy polymers. Part II: Thermal analysis. Mechanics of Materials, 32(3):149–159, 2000.
14. A. Benaarbia, A. Chrysochoos, and G. Robert. Kinetics of stored and dissipated energies associated with cyclic loadings of dry polyamide 6.6 specimens. Polymer Testing, 34:155–167, 2014.
15. A. Benaarbia, A. Chrysochoos, and Gilles Robert. Influence of relative humidity and loading frequency on the pa6.6 thermomechanical cyclic behavior: Part ii. energy aspects. Polymer Testing, 41:92 – 98, 2015.
16. J. Gough, A description of a property of caoutchouc or india rubber (letter to Dr Holme written in 1802). Proc Lit and Phil Soc Manchester, 2nd, ser. 1, 288, 1805
17. .J. P. Joule. On some thermodynamic properties of solids. Phil Mag 4th, 14:227, 1857.
18. R. Clausius. Sur diverses formes facilement applicables qu'on peut donner aux equations fondamentales de la théorie mécanique de la chaleur (traduced from German by H.-F. Bessard). Journal de mathématiques pures et appliquées 2ème série, 10:361–400, 1865.
19. H. Bouasse and Z. Carrière. Courbes de traction du caoutchouc vulcanisé. Annales de la Faculté des Sciences de Toulouse, 5:257–283, 1903.
20. W. L. Holt. Behavior of rubber under repeated stresses. Journal of Industrial and Engineering Chemistry, 23:1471–1475, 1931.
21. L. Mullins. Effect of stretching on the properties of rubber. Rubber Chemistry and Technology, 21:281– 300, 1948.
22. S. M. Cadwell, R. A. Merril, C. M. Sloman, and F. L. Yost. Dynamic fatigue life of rubber. Industrial and Engineering Chemistry (reprinted in Rubber Chem. and Tech. 1940;13:304-315), 12:19–23, 1940.
23. J. H. Fielding. Flex life and crystallisation of synthetic rubber. Industrial and Engineering Chemistry, 35(12):1259–1261, 1943.
24. R. S. Rivlin and A. G. Thomas. Rupture of rubber. I.Characteristic energy for tearing. Journal of Polymer Science, 10:291–318, 1953.
25. A. G. Thomas. Rupture of rubber - vi - further experiments on the tear criterion. Journal of Polymer Science, 3:168–174, 1960.
26. R Stoček, G Heinrich, R Kipscholl, O Kratina, (2021). Cut & chip wear of rubbers in a range from low up to high severity conditions, Applied Surface Science Advances, 6 (1), 100152, https://doi.org/10.1016/j.apsadv.2021.100152
27. N. Saintier, G. Cailletaud and R. Piques. Cyclic loadings and crystallization of natural

rubber: An explanation of fatigue crack propagation reinforcement under a positive loading ratio. Mater. Sci. Eng. A. 2011;528(3):1078–1086.
28. G.L. Clark, M. Kabler, E. Blaker and JM Ball. Hysteresis in crystallization of stretched vulcanized rubber from X-ray data. Industrial and Engineering Chemistry 32: 1474-1477, 1940.
29. T. Rey, G. Chagnon, J.-B. Le Cam and D. Favier. Influence of the temperature on the mechanical behaviour of filled and unfilled silicone rubbers. Polymer Testing, 32: 492-501, 2013.
30. D. Göritz and F. H. Müller. Die kalorimetrische erfassung der dehnungskristallisation polymerer. Kolloid-Zeitschrift und Zeitschrift für Polymere, 241(20):1075–1079, 1970.
31. J. C. Mitchell and D. J. Meier. Rapid stress-induced crystallization in natural rubber. Journal of Polymer Science Part A-2: Polymer Physics, 6(10):1689–1703, 1968.
32. Dedova, S. and Schneider, K. Characterisation of Crack Propagation in Natural Rubber Under Complex Loading Conditions Using Thermographic Methods. In: Advances in Polymer Science. Springer, Berlin, Heidelberg. https://doi.org/10.1007/12_2023_164, 2023.
33. F.P. Wolf and G. Allen. Polymer, 16:209, 1975.
34. G. Allen, U. Bianchi, and C. Price. Trans. Faraday Soc., 59:2493, 1963.
35. G. Allen, M.J. Kirkham, J. Padget, and C. Price. Trans. Faraday Soc., 67:1278, 1971.
36. M.C. Shen. Macromolecules, 2:358–364, 1969.
37. M. Shen and M. Croucher. Contribution of internal energy to the elasticity of rubberlike materials. Polymer Reviews, 12:287–329, 1975.
38. L R G Treloar. The elasticity and related properties of rubbers. Reports on Progress in Physics, 36(7):755, 1973.
39. L. R. G. Treloar. The Physics of Rubber Elasticity. Oxford University Press, Oxford, 1975.
40. G. Heinrich, M. Kaliske, M. Klüppel, J.E. Mark, E. Straube, and T.A. Vilgis. The thermoelasticity of rubberlike materials and related constitutive laws. Journal of Macromolecular Science. Part A., 40:87–93, 2003.
41. C. Price. Thermodynamics of rubber elasticity. Proc R Soc Lond A, 351:331–350, 1976.
42. J.E. Mark. Thermoelastic Properties of Rubber like Networks and Their Thermodynamic and Molecular Interpretation. Rubber Chemistry and Technology, 46(3):593–618, 07 1973.
43. Ulf W. Gedde. Chapter 3: The Rubber Elastic State, pages 39–53. Springer Netherlands, Dordrecht, 1999.
44. G. Heinrich. Thermoelasticity of Rubbers. Springer Berlin Heidelberg, Berlin, Heidelberg, 2014.
45. V. Honorat. Analyse thermomécanique par mesure de champs des élastomères. PhD thesis, Sciences et techniques du Languedoc. Montpellier, Université Montpellier 2, 2006.
46. R. L. Anthony, R. H. Caston, and E. Guth. Equations of state for naturals and synthetic rubber like materials: unaccelerated natural soft rubber. Journal of Physical Chemistry,

46:826, 1942.
47. R. Caborgan. Contribution à l'analyse expérimentale du comportement thermomécanique du caoutchouc naturel. PhD thesis, 2011. Mécanique et Génie civil Montpellier 2.
48. J. R. Samaca Martinez, J.-B. Le Cam, X. Balandraud, E. Toussaint, and J. Caillard. Mechanisms of deformation in crystallizable natural rubber. Part 2: quantitative calorimetric analysis. Polymer, 54:2727-2736, 2013.
49. J. R. Samaca Martinez, J.-B. Le Cam, X. Balandraud, E. Toussaint, and J. Caillard. Filler effects on the thermomechanical response of stretched rubbers. Polymer testing, 32:835-841, 2013.
50. J. R. Samaca Martinez, J.-B. Le Cam, X. Balandraud, E. Toussaint, and J. Caillard. New elements on Mullins effect: a thermomechanical analysis. European Polymer Journal, 55:98–107, 2014.
51. J.-B. Le Cam. Energy storage due to strain-induced crystallization in natural rubber: the physical origin of the mechanical hysteresis. Polymer, 127:166–173, 2017.
52. J. B. Le Cam, Jose Ricardo Samaca Martinez, X. Balandraud, E. Toussaint, and J. Caillard. Thermo-mechanical Analysis of the Singular Behavior of Rubber: Entropic Elasticity, Reinforcement by Fillers, Strain-Induced Crystallization and the Mullins Effect. Experimental Mechanics, 55(4):771–782, 2015.
53. A. Lachhab, E. Robin, J.-B. Le Cam, F. Mortier, Y. Tirel, and F. Canevet. Energy stored during deformation of crystallizing TPU foams. Strain, e12271, 2018.
54. M.T. Loukil, G. Corvec, E. Robin, M. Miroir, J.-B. Le Cam, and P. Garnier. Stored energy accompanying cyclic deformation of filled rubber. European Polymer Journal, 98:448 – 455, 2018.
55. J.-B. Le Cam. Strain-induced crystallization in rubber: A new measurement technique. Strain, 54(1):e12256, 2018.
56. J B. Le Cam, P.-A. Albouy, and S. Charlès. Comparison between X-ray diffraction and quantitative surface calorimetry based on IR thermography to evaluate strain-induced crystallinity in natural rubber. Submitted to Review of Scientific Instruments, 91:044902, 2020.
57. J.-B. Le Cam, W.A. Kyei-Manu, A. Tayeb, P.-A. Albouy, J. J. C. Busfield, and L. B. Tunnicliffe. Strain-induced crystallisation of reinforced elastomers using surface calorimetry, 131: 108341, 2023.
58. J.-B. Le Cam, A. Tayeb and S. Charlès. First evidence and characterization of strain-induced crystallization heterogeneity in natural rubber under homogeneous strain states. Polymer, 255:125120, 2022.
59. S. Charlès and J.-B. Le Cam. Inverse identification of constitutive parameters from heat source fields: A local approach applied to hyperelasticity. Strain, 56(2), 2020.
60. E. Toussaint, X. Balandraud, J.-B. Le Cam, and M. Grédiac. Combining displacement, strain, temperature and heat source fields to investigate the thermomechanical response of an elastomeric specimen subjected to large deformations. Polymer Testing, 31(7):916 – 925, 2012.
61. V.N. Khiem, J.-B. Le Cam, S. Charlès and M. Itskov. Thermodynamics of strain-induced

crystallization in filled natural rubber under uni- and biaxial loadings, part 1: Complete energetic characterization and crystallinity evaluation. Journal of the Mechanics of the Mechanics of the Mechanics and Physics of Solids, 159: 104701, 2022.

62. T. Pottier, M.-P. Moutrille, J.-B. Le Cam, X. Balandraud, and M. Grédiac. Study on the use of motion compensation technique to determine heat sources. application to large deformations on cracked rubber specimens. Experimental Mechanics, 49:561–574, 2009.
63. J. R. Samaca Martinez, X. Balandraud, E. Toussaint, J. B. Le Cam, and D. Berghezan. Thermomechanical analysis of the crack tip zone in stretched crystallizable natural rubber by using infrared thermography and digital image correlation. Polymer, 55(24):6345–6353, 2014.
64. J. R. Samaca Martinez, E. Toussaint, X. Balandraud, J. B. Le Cam, and D. Berghezan. Heat and strain measurements at the crack tip of filled rubber under cyclic loadings using full-field techniques. Mechanics of Materials, 81:62–71, 2015.
65. J. B. Le Cam, J. Trubert, S. Charlès, R. Fernandes and V. Lemos. Thermomechanical and calorimetric characterization of crack tip zones under large heterogeneous deformations, Part II: Full strain, calorimetric and strain-induced crystallinity fields at the crack tip of an unfilled natural rubber. Polymer, 341:129183, 2025.
66. H. Louche. Etudes de certains phénomènes de localisation à partir de champs thermomécaniques. Habilitation thesis, Savoie University, 2009.
67. E. Verron and A. Andriyana. Definition of a new predictor for multiaxial fatigue crack nucleation in rubber. Journal of the Mechanics and Physics of Solids, 56(2):417 – 443, 2008.
68. H. Baaser, C. Hopmann, and A. Schobel. Reformulation of strain in variants at incompressibility. Archive of Applied Mechanics, 83:273–280, 2013.
69. A. Chrysochoos. Analyse du comportement des matériaux par thermographie infra rouge. In Colloque Photomécanique, volume 95, pages 201–211, 1995.
70. B. Berthel, A. Chrysochoos, B. Wattrisse, and A. Galtier. Infrared image processing for the calorimetric analysis of fatigue phenomena. Experimental Mechanics, 48:79–90, 2008.
71. A. Chrysochoos and H. Louche. An infrared image processing to analyse the calorific effects accompa- nying strain localisation. Int J Eng Sci, 38:1759–1788, 2000.
72. X. Balandraud, A. Chrysochoos, S. Leclercq, and R. Peyroux. Influence of the thermomechanical coupling on the propagation of a phase change front. C R Acad Sci - Series IIB - Mechanics, 329:621– 626, 2001.
73. F. Maquin and F. Pierron. Heat dissipation measurements in low stress cyclic loading of metallic materials: From internal friction to micro-plasticity. Mechanics of Materials, 41:928–942, 2009.
74. G. A. Maugin and W. Muschik. Thermodynamics with Internal Variables. Part I. General Concepts. Journal of Non-Equilibrium Thermodynamics, 19: 217-249, 1994.
75. C.W. Bunn. Proc. R. Soc. London, Ser. 1, 180:40, 1942.
76. Y. Takahashi and T. Kumano. Crystal Structure of Natural Rubber. Macromolecules, 37:4860, 2004.

77. A. Immirzi, C. Tedesco, G. Monaco, and A.E. Tonelli. Crystal Structure and Melting Entropy of Natural Rubber. Macromolecules, 38:1223, 2005.
78. G. Rajkumar, J.M. Squire, and S. Arnott. Macromolecules, 39:7004, 2006.
79. S. Toki, I. Sics, S.F. Ran, L.Z. Liu, B.S. Hsiao, S. Murakami, M. Tosaka, S. Kohjiya, S. Poompradub, Y. Ikeda, and A.H. Tsou. Rubber Chemistry and Technology, 42:956–964, 2004.
80. S. Toki, T. Fujimaki, and M. Okuyama. Strain-induced crystallization of natural rubber as detected real-time by wide-angle x-ray diffraction technique. Polymer, 41:5423–5429, 2000.
81. S. Trabelsi, P.-A. Albouy, and J. Rault. Effective local deformation in stretched filled rubber. Macromolecules, 36:9093–9099, 2003.
82. Donald E. Roberts and Leo Mandelkern. Thermodynamics of crystallization in high polymers. natural rubber. Rubber Chemistry and Technology, 28(3):718–727, 1955.
83. J. R. Samaca Martinez, J.-B. Le Cam, X. Balandraud, E. Toussaint, and J. Caillard. Mechanisms of deformation in crystallizable natural rubber. Part 1: Thermal characterization. Polymer, 54:2717-2726, 2013.
84. J.-B. Le Cam. Fast evaluation and comparison of the energy performances of elastomers from relative energy stored identification under mechanical loadings. Polymers, 14(3), 2022.
85. L. Mullins. Permanent set in vulcanized rubber. Rubber Chemistry and Technology, 22(4):1036–1044, 1949.
86. L. Mullins. Softening of rubber by deformation. Rubber Chemistry and Technology, 42:339–362, 1969.
87. Gerhard-A Holzapfel. Non linear solid mechanics - a continuum approach for engineering. Wiley, 2000.
88. P. D'Ambrosio, D. De Tommasi, D. Ferri, and G. Puglisi. A phenomenological model for healing and hysteresis in rubber-like materials. International Journal of Engineering Science, 46(4):293–305, 2008.
89. A Dorfmann and RW Ogden. A pseudo-elastic model for loading, partial unloading and reloading of particle-reinforced rubber. International Journal of Solids and Structures, 40(11):2699–2714, 2003.
90. T. Rey, G. Chagnon, D. Favier, and J.-B. Le Cam. Hyperelasticity with rate-independent microsphere hysteresis model for rubberlike materials. Computational Materials Science, 90:89 – 98, 2014.
91. A. Vandenbroucke, H. Laurent, N. Ait Hocine, and G. Rio. A Hyperelasto-Visco-Hysteresis model for an elastomeric behaviour: Experimental and numerical investigations. Computational Materials Science, 48(3):495–503, 2010.
92. V. Le Saux, Y. Marco, S. Calloch, C. Doudard, and P. Charrier. Fast evaluation of the fatigue life-time of rubber-like materials based on a heat build-up protocol and micro-tomography measurements. International Journal of Fatigue, 32(10):1582-1590, 2010.
93. C. Ovalle Rodas, F. Zaïri, M. Naït-Abdelaziz, and P. Charrier. A thermo-visco-hyperelastic model for the heat build-up during low-cycle fatigue of filled rubbers:

Formulation, implementation and experimental verification. International Journal of Plasticity, 79:217–236, 2016.
94. O. Peter, R. Stoček, and O. Kratina. Experimental and Numerical Description of the Heat Build-Up in Rubber Under Cyclic Loading. Springer International Publishing, Cham, Heinrich, Gert and Kipscholl, Reinhold and Stoček, Radek, 2023.
95. P.H. Mott, C.B. Giller, D. Fragiadakis, D.A. Rosenberg, and C.M. Roland. Deformation of polyurea: Where does the energy go? Polymer, 105:227 – 233, 2016.
96. V.N. Khiem, J.-B. Le Cam, S. Charlès and M. Itskov. Thermodynamics of strain-induced crystallization in filled natural rubber under uni- and biaxial loadings, Part II: Physically-based constitutive theory. Journal of the Mechanics of the Mechanics of the Mechanics and Physics of Solids, 159: 104712, 2022.
97. L. R. G. Treloar. Stress-strain data for vulcanised rubber under various types of deformation. Transactions of the Faraday Society, 40:59-70, 1944.
98. I. M. Ward and D. W. Hadley, An introduction to the mechanical properties of solid polymers. John Wiley and Sons Ltd, New-York, 2nd Ed., 1993.
99. C. G'Sell and A. Coupard. Génie mécanique des caoutchoucs. Appollor et INPL. Ecole des Mines de Nancy, ISBN 2-9510704-0-3, 1997.
100. M. Sasso, G. Palmieri, G. Chiappini, D. Amodio. Characterization of hyperelastic rubber-like materials by biaxial and uniaxial stretching tests based on optical methods. Polymer Testing, 27: 995-1004, 2008.
101. N. Promma, B. Raka, M. Grédiac, E. Toussaint, J.-B. Le Cam, X. Balandraud and F. Hild, Application of the virtual fields method to mechanical characterization of elastomeric materials, International Journal of Solids and Structures, 46:698-715, 2009.
102. T. Guélon, E. Toussaint, J.-B. Le Cam, N. Promma and M. Grédiac. A new characterization method for rubbers. Polymer Testing, 28: 715-723, 2009.
103. M. Johlitz and S. Diebels. Characterisation of a polymer using biaxial tension tests. part I: Hyperelasticity. Arch Appl. Mech, 81: 1333-1349, 2011.
104. H. Seibert, T. Scheffer and S. Diebels. Testing of Elastomers - Experimental Setup, Measurement and Experimental Optimisation of Specimen's Shape. Technische Mechanik, 81: 72-89, 2014.
105. J. Trubert, J.-B. Le Cam, S. Charlès, R. Fernandes and V. Lemos. Thermomechanical and calorimetric characterization of crack tip zones under large heterogeneous deformations, Part I: A method coupling full kinematic and thermal fields for high resolution surface micro-calorimetry. Polymer, 342:129286, 2026.
106. J.-B. Le Cam, S. Charlès. Maximum principal stretch field at a stretched unfilled natural rubber crack tip (30 April 2021). Mendeley data, DOI:10.17632/3ymcjp78xn.1, 2025.
107. J.-B. Le Cam, S. Charlès. Thermal field at a stretched unfilled natural rubber crack tip (30 April 2021). Mendeley data V1, DOI:10.17632/t26jxyzrgj.1, 2025.
108. J.-B. Le Cam, S. Charlès. Heat source field at a stretched unfilled natural rubber crack tip (30 April 2021). Mendeley data V1, DOI:10.17632/jgmgm3t43t.1, 2025.
109. J.-B. Le Cam, S. Charlès. Crystallinity field at a stretched unfilled natural rubber crack

tip from surface calorimetry (4 May 2021). Mendeley data V1, DOI:10.17632/njnkpjjdsk.1, 2025.

110. F. Xiang, K. Schneider, M. Schwartzkopf, G. Heinrich. Competition between strain-induced crystallization and cavitation at the crack tip of unfilled and carbon black-filled natural rubber more. Macromolecules, 55:10682–93, 2022.
111. G. Heinrich, R. Kipscholl, J.-B. Le Cam, and R. Stoček, editors. Advances in Understanding Thermal Effects in Rubber: Experiments, Modelling, and Practical Relevance, volume 294 of Advances in Polymer Science. Springer Nature Switzerland, Cham, 2024.
112. R. Osumi, T. T. Mai, K. Tsunoda and K. Urayama. Pronounced effect of strain biaxiality on high-temperature behavior of strain-crystallizing elastomers. Soft Matter, 21:5080-5088, 2025.
113. D. Nozaki, T. T. Mai, K. Tsunoda and K. Urayama. Tracking the Evolution of Heterogeneous Crystallization Driven by Complex Deformation Scenarios in Natural Rubber. Macromolecules, 58:4059-4069, 2025.
114. T. T. Mai, D. Nozaki, Y. Tokudome, K. Tsunoda and K. Urayama. Coupled Evolution of Local Stress and Strain-Induced Crystallization Near a Circular Defect in Stretched Natural Rubber. Macromolecules, 59:1568-1580, 2026.